Mineralogy, sedimentology and physical properties of two sediment cores from the Southern Tasman Sea (SW Pacific Sector)

Diploma Thesis

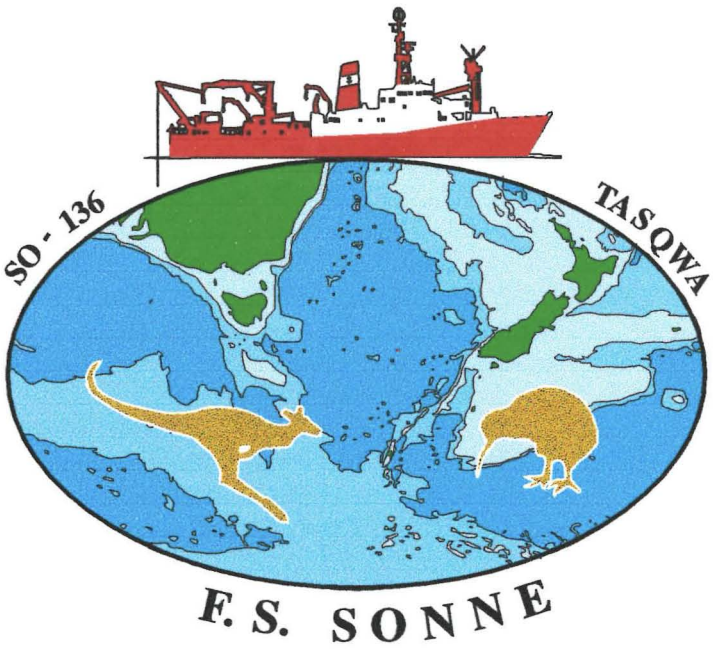

Mathematisch-Naturwissenschaftliche Fakultät
der
Christian-Abrechts-Universität
zu Kiel

submitted by
Sven Roth
Kiel, July 1999

Frontispiece:
TASQWA logo of the RV SONNE cruise SO136 from Wellington (New Zealand) to Hobart (Tasmania, Australia) during October and November 1998, created by Dr. Stefan Nees.

Hiermit versichere ich, daß ich die vorliegende Arbeit selbständig und nur mit den im Text, sowie im Literaturverzeichnis erwähnten Hilfsmitteln verfaßt habe.

Diese Diplomarbeit wurde im Rahmen des TASQWA Projektes durchgeführt. Da es sich dabei um ein internationales Projekt handelt, wurde diese Arbeit in Absprache mit der Vorsitzenden des Prüfungsausschusses, Frau Prof. Dr. P. Schäfer, in englischer Sprache verfaßt.

Kiel, im Juli 1999

_____

Sven Roth

ABSTRACT

This thesis was compiled as part of the TASQWA project (Quaternary variability of water masses in the Southern Tasman Sea and the Southern Ocean, SW Pacific Sector). The aim of this project is to investigate Quaternary changes of water masses in the Tasman Sea and the Southern Ocean.
Paleoclimatic and paleoceanographic changes will be reconstructed using micropaleontological, mineralogical, sedimentological and oceanographic methods.
The studied area is the South Tasman Rise (STR), located south off Tasmania, Australia and its southern extension. Although this ocean area is thought to play a major key-role for the global ocean circulation, connecting the world oceans (as part of the "Global Ocean Convejor Belt"), this specific region is poorly investigated.
The goal of this thesis was to perform mineralogical and sedimentological investigations of two sediment cores which were retrieved from this area during the RV SONNE cruise SO136 from Wellington (New Zealand) to Hobart (Tasmania, Australia) in October and November 1998.
The two cores investigated show distinct lithologies, mineralogies and sedimentologies, controlled by different bathymetric conditions as well as different biological, physical and chemical oceanic processes during the late Quaternary.
Core SO136-155GC was retrieved from the eastern flank of the South Tasman Rise (lat.: 47°00.09S, long.: 149°31.30E) at 3170m water depth. It shows high sedimentation rates (2-2.5cm/ka) and dominance of carbonates (81-91%) throughout the entire core. The core position is located within the Subantarctic Zone and the northward shift of the oceanic frontal system during glacial stages obviously had no major effect on the nature of the sediments. Dissolution patterns are controlled by fluctuations of the CO_2 partial pressure due to increased input of organic matter during the interglacials and less input during the glacials, respectively. In addition, a series of turbidites was found within this sediment core.
The manganese rich (manganese pavement and two buried horizons) sediment core SO136-124GC was gathered south of the South Tasman Rise (lat.: 52°59.77S, long.:151°08.14E) at 4141m water depth. With 0.8-2.3cm/ka, sedimentation rates are distinctly lower. The sediments are dominated by terrigenic components, which are derived from the bathymetric high west of the core position (> 1000m difference in altitude), due to the erosional effect of westerly bottom and deep water currents. The biogenic fraction of the sediments show a clear interglacial to glacial pattern, presumably created by the northward shift of the oceanic frontal system. Due to the northward shift of the Polar Front within the glacials, the core position was under the influence of the Antarctic opal belt, whereas carbonate production was increased (> 50% carbonate content) during the interglacials, when the core position was south of the Subantarctic Front. Several levels of carbonate crusts within this core are an interesting feature. Three models are proposed to explain their genesis.
The occurrence of numerous dropstones mark the melting phases of the outgoing glacials and allow to postulate iceberg drifts as known from the northern hemisphere.
The large discrepancies between the investigated cores indicate that the Australian sector of the Southern Ocean is a highly complex ocean region with respect to biological, physical and chemical processes and their sedimentological signals.

TABLE OF CONTENTS

the Antarctic continent's climate and can be traced into the northern hemisphere of all ocean basins, e.g. up to the latitude of the New Foundland Rise, 40°N in the Atlantic Ocean (Dietrich et al., 1975). In contrast, North Atlantic Deep Water (NADW), formed in the Arctic Ocean, flows down south and is forced to rise in between 40° and 50°S to become part of the Antarctic Circumpolar Current (ACC). The ACC is the world's most powerful current flowing around Antarctica and extending north up to the Subantarctic Front (SAF). Important passages of water mass exchange and heat transfer between the Indian and Pacific oceans are also located around Australia. Therefore, the aim of the TASQWA project is to evaluate the changing oceanographic settings of the Late Quaternary and, as a result, to provide a better understanding of global climatic changes.

Within the TASQWA project, investigations of fossil remains of planktic and benthic organisms (foraminifers, ostracoda, diatoms, radiolarian, dinoflagellates, cysts. molluscs and gastropods), as well as sedimentological studies (carbonate mineralogy and grain size distribution) were performed. In addition, geophysical methods, like an echo sounder and a side scan sonar, were deployed in order to support the interpretation of the sediments and depositional features (by swath bathymetry and seismic data).

To achieve most effective results, the TASQWA project was planned as a joint venture research program in which, besides the German scientific crew, scientists and scientific research departments from Australia, New Zealand and France are involved.

1.2. THE RV SONNE CRUISE SO136

During the German Research Vessel (RV) SONNE 136 cruise from Wellington to Hobart (16th of October - 12th of November), a total of 24 sediment cores were taken (9 of which were empty) with a total length of 103.05m.

On October the 16th, 1998 at 08:00pm local time, the RV SONNE left the harbour of Wellington/New Zealand, to reach station N° 1, located north-west off the southern Island of New Zealand. The first objective was to construct a profile across the Challenger Plateau (location see figure 1-2). At this transect (17th and

18th of October) the first two gravity cores (GC) were successfully taken (site 1 & 2).

After finishing the transect across the Campbell Plateau on the 30th of October, whereby the gravity corer was deployed 11 times, the SONNE entered the Emerald Basin (for locations see figure 1-2). Only five coring attempts were successful due to the coarse nature of the sediment (the gravity corer could not penetrate properly).

The sediment core SO136-117GC with a total length of 10.69m was taken on the 1st of November at the last station of the Emerald Basin-transect (site 21, see figure 1-2). This core shows some distinct colour changes and the sediments were distinctly different to the diatomaceous oozes and muds found approximately 50 nautical miles south of this station (site 20, core SO136-111GC).

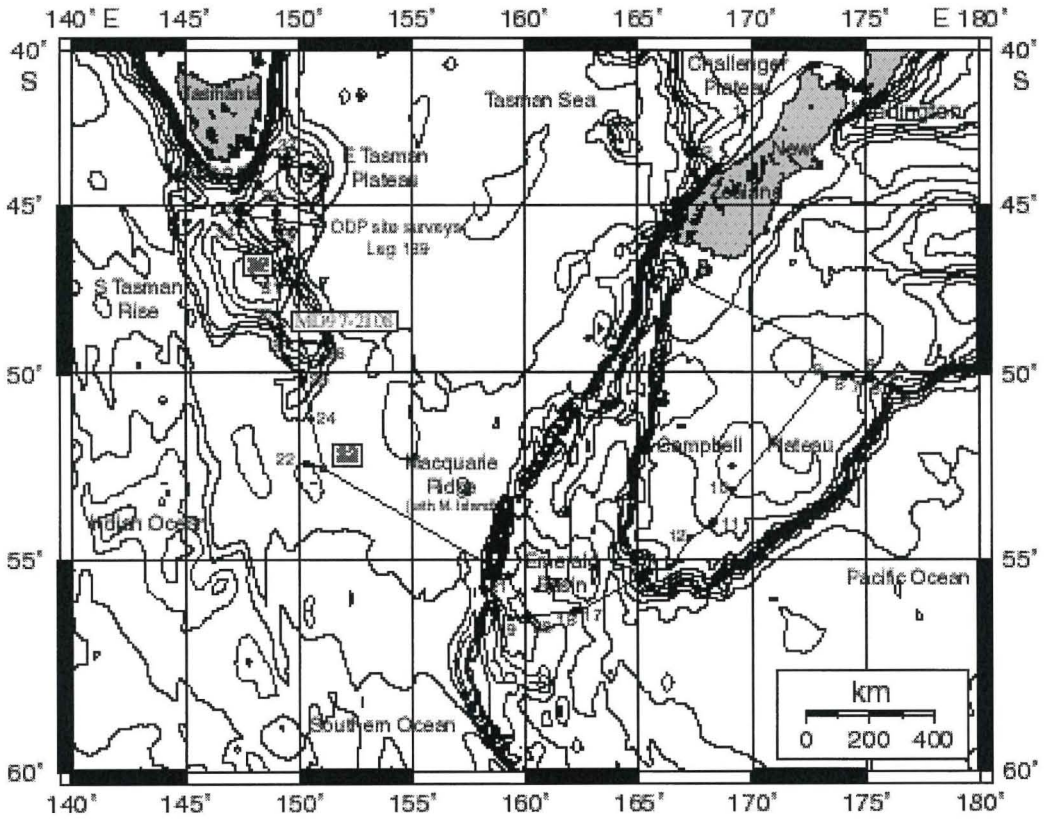

Fig. 1-2: Cruise track of the TASQWA-SO136 expedition, including the locations of sampled stations and ODP site surveys.

During the last transect, crossing the South Tasman Rise, both of the sediment cores investigated within this thesis were recovered. The first one, SO136-124GC out of a depth of around 4200m was retrieved at the beginning of the transect at site 23, station 124 (see figure 1-2). The other core (SO136-155GC) is one of the last cores, taken during this cruise on the 8th of November and was taken at a waterdepth of 3200m (site 32, station155), which explains the good carbonate preservation (80-90% carbonate content) throughout this core (for the exact positions see chapter 3.1.1. CORE LOCATIONS).

The specific distribution of the core locations was chosen, to get a vertical and horizontal North - South - depth profile over the South Tasman Rise and to compare and thus evaluate differences of the sedimentological features and the mineralogy of these two sediment cores.

The cores studied are near the MD97-2108 core, taken during the IMAGES III IPHIS expedition in 1997 with the French RV MARION DUFRESNE. (Suhonen, 1998, which included sedimentological and mineralogical analysis).

1.3. RESEARCH HISTORY

A large data set, comprising seismic and sedimentological data were gathered during numerous cruises of R.V. VEMA and R.V. ROBERT D. CONRAD, in the late sixties and early seventies (Hayes, 1971).

During several cruises in the time period from 1968 to 1971, the USNS Eltanin recovered over 300 piston cores in the Indian Ocean region between Australia and Antarctica. Conolly (1971) used these cores to establish an overview of the physiography and the sediment thickness, as well as the distribution of surface sediment types on the southern and south-eastern side of the South Tasman Rise. Conolly & Payne (1971) mapped the manganese pavement of the South Tasman Rise by bottom photography.

More data from cores taken during cruises with the research vessels of Lamont-Doherty Geological Observatory in the Indian Ocean region and south of Australia were discussed by Opdyke and Glass (1969).

The first seismic survey including the Tasmanian Region was achieved by the Bureau of Mineral Resources (BMR) Continental Margins Survey in 1972 using a 120 kilojoule sparker source (Tilbury,1974). Willcox (1978) used these data to write a report on the Australian southern margin.

In 1973, under supervision of the BMR (Bureau of Mineral Resources), the R.V. SPRIGHTLY gathered a low-energy sparker profile of the West Tasmanian shelf over 1000km, approximately. The profiles displayed the stratigraphy of the sediments down to the late Miocene. Surface sediment samples taken on the same cruise showed the quartz sand coverage (including some shell debris) of the inner shelf area, whereas the outer shelf was covered by medium to coarse grained bryozoal sand and gravel (Jones & Davies, 1983).

During the RV GLOMAR CHALLENGER expedition in 1973, participants of the Deep Sea Drilling Project (DSDP, Leg 29) drilled four holes in the Tasmanian region. Two of these cores, sites 280 and 281, located slightly west of the SE - NW trending profile are discussed in the AGSO (Australian Geological Survey Organisation) Cruise 147 Report (1995/96). According to the AGSO REPORT 1995/96, the bottom of core 281 was radiometrically dated as late Carboniferous (305 Ma).

During the year 1985, the Federal Institute for Geosciences and Natural Resources (BGR, Hannover, Germany) in co-operation with the BMR, undertook two expeditions with the German R.V. SONNE in this region. The first cruise, SO36 (2nd Leg), gathered geophysical data on the western side of Tasmania and on the Southern Tasman Rise, while the second cruise, SO36 (3rd Leg), also collected samples in this area. Some of the dredged samples are thought to be older than Tertiary. A detailed report of the research results is published by Hinz et al. (1985).

In order to detect new potential petroleum deposits, the BMR Cruise 67 was carried out west off the Tasmanian margin on the R.V. RIG SEISMIC. The aim of

this expedition was to get new geological, geochemical and heatflow data (Exon & Lee, 1987; Exon et al., 1992).

In 1994 the Australian Geological Survey Organisation (AGSO), successor of the BMR, undertook a swath-mapping-cruise with the French R.V. L'ATALANTE, during which approximately 200,000 km^2 of the oceanfloor west and south of Tasmania were surveyed (Exon et al., 1994).

During the IMAGES III IPHIS cruise in May 1997 from Hobart/Tasmania to Christchurch / New Zealand, with the French R.V. MARION DUFRESNE, a total of 19 sediment cores were retrieved, 3 of which are located at the South Tasman Rise. The aim of the IMAGES-project was to provide a detailed, world wide study of the global palaeoceanographic and palaeoclimatical changes during the last 500,000 years (Nees et al., 1998).

2. OCEANOGRAPHIC AND GEOLOGICAL BACKGROUND

2.1. ATHMOSPHERIC CIRCULATION

A major part of the Southern Ocean is located in the West Wind Drift Zone and therefore is under the influence of strong westerly winds. Due to the fact that there is no land barrier reducing the wind speeds around Antarctica, heavy storms are very common. Because of little variations in wind directions, the windstress acting on the water surface results in very high waves.

This is the major process driving the world's strongest ocean current, the Antarctic Circumpolar Current.

Figure 2-1 shows the annual variability of the atmospheric circulation in the Southern Ocean off Australia and New Zealand.

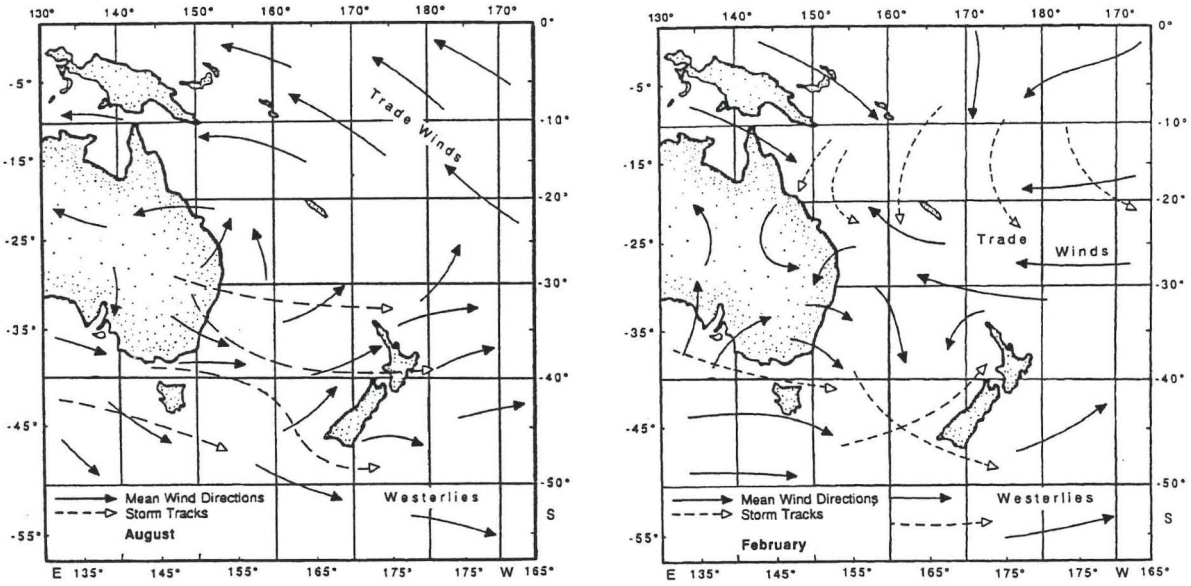

Fig.2-1: Present-day surface wind system and major storm tracks over the Southwest Pacific Ocean during austral winter and austral summer. (After Schott, 1935a; Gentilli, 1971; Wyrtki and Meyers, 1975)

The West Wind Drift Zone extends from ca 30°S to around 60°S. South of this latitude easterly winds dominate, creating the westward flow of the Polar Current.

Wind changes during the Last Glacial Maximum (LGM)

Using the distribution of aeolian quartz in the Tasman Sea, Thiede (1979) showed that the westerly winds over the Southwest Pacific had shifted to the north due to the influence of intensified atmospheric circulation during the Last Glacial Maximum (see figure 2-2).

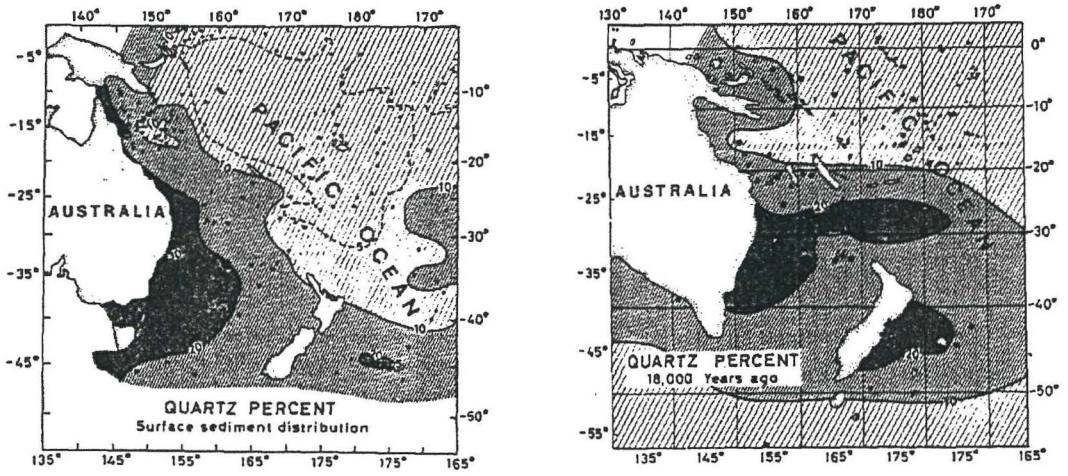

Fig.2-2: Aeolian quartz input from the Australian Continent during the Holocene and during the LGM. The southward shift of the aeolian quartz input distribution during the LGM is marked by dark grey colours. (From Thiede, 1979)

Klinck and Smith (1993) introduced a model, describing the atmosphere to ocean surface interaction during the LGM. Their model supports an increased transport of the Antarctic Circumpolar Current (ACC) as result of higher wind speeds, accelerating the surface currents. This and shifted positions of wind stress may have caused the northward shift of the oceanic front system during the LGM (for details see Klinck and Smith, 1993).

Except for the horizontal component, the overall mass transport of the ACC contains several vertical components which cause the frontal system of the Southern Ocean. Reid and Nowlin (1971) measured an overall water transport of 237 Sv through the Drake Strait which by far is the biggest water transport ever measured world-wide. Therefore, the ACC is the most powerful ocean current in the world.

Modern circulation within the Australian sector of the Southern Ocean is characterised by three major oceanic fronts. The Polar Front Zone (PF), the Subantarctic Front (SAF) and the Subtropical Front (STF) (see fig. 2-4).

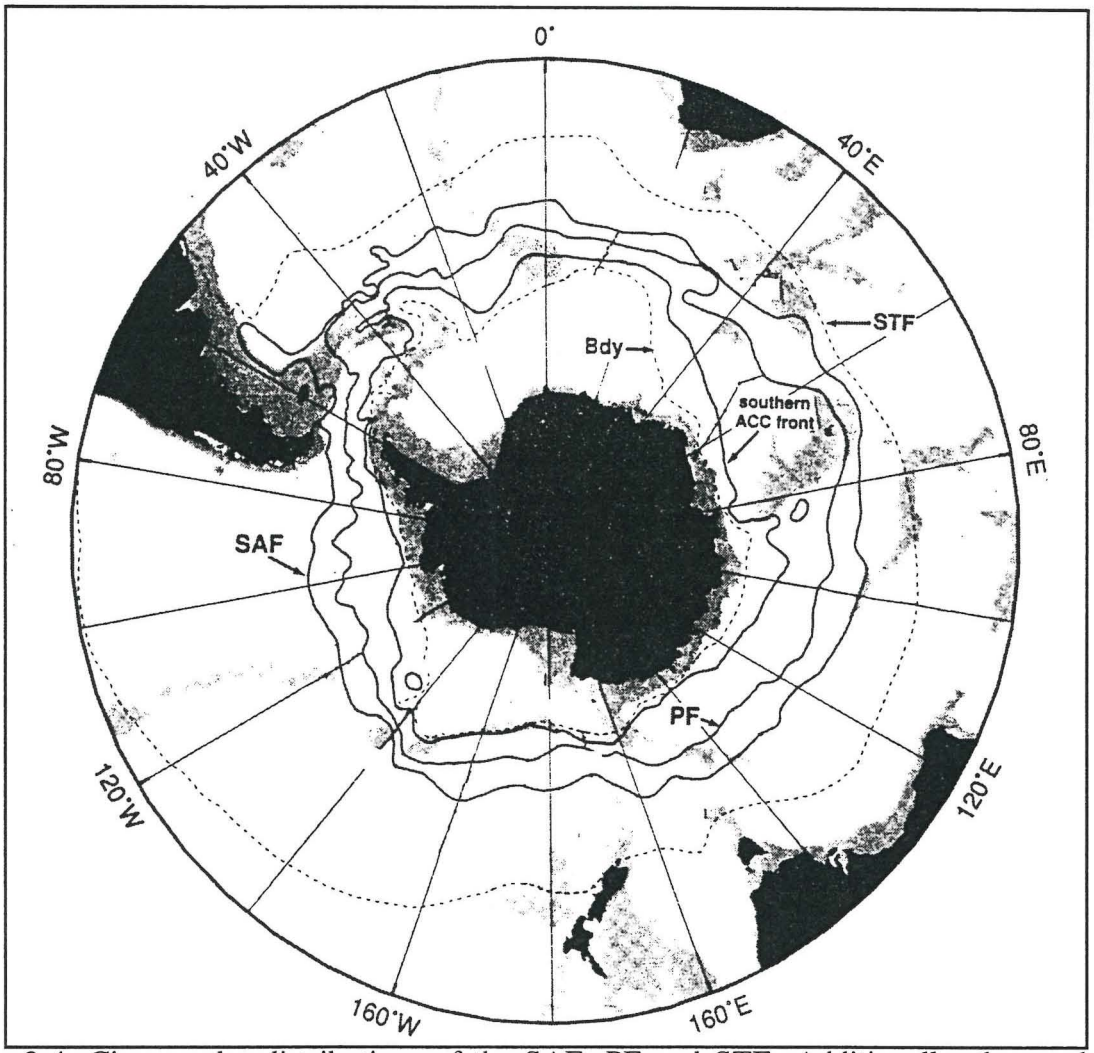

Fig. 2-4: Circumpolar distributions of the SAF, PF and STF. Additionally, the southern boundary of the ACC is shown. (After Orsi et al., 1995)

The STF, only interrupted by South America, marks the northernmost extent of Subantarctic Waters. The STF separates the waters of the Southern Ocean from the warmer and saltier waters of the circulation's of the subtropical regions. This zone

is identified by a strong temperature gradient between 10°-14°C in winter and 14°-18°C in summer.

In the Australian sector of the southern Ocean, the STF forms the boundary between the Subantarctic Current and the Tasman current and extends along ~45°S, following the 15°C surface summer isotherm, the 10° C winter isotherm and the 34.7- 34.8 salinity isoplethe (Garner, 1959).

As the modern STF and the Polar Front Zones are well delineated by SST gradients, their position in the past can be inferred from surface water paleotemperatures by statistical analysis of the composition of the planktonic foraminifer population (Wells and Connell, 1997).

Both the Subantarctic Front and the Polar Front together mark the transition between Subantarctic and Antarctic water masses and show a seasonal variability between 53°-55°S.

Figure 2-5 shows the present day surface circulation in the Tasman Sea and the oceanic fronts. The Subtropical Convergence marks the northernmost border of the Antarctic Circumpolar Current.

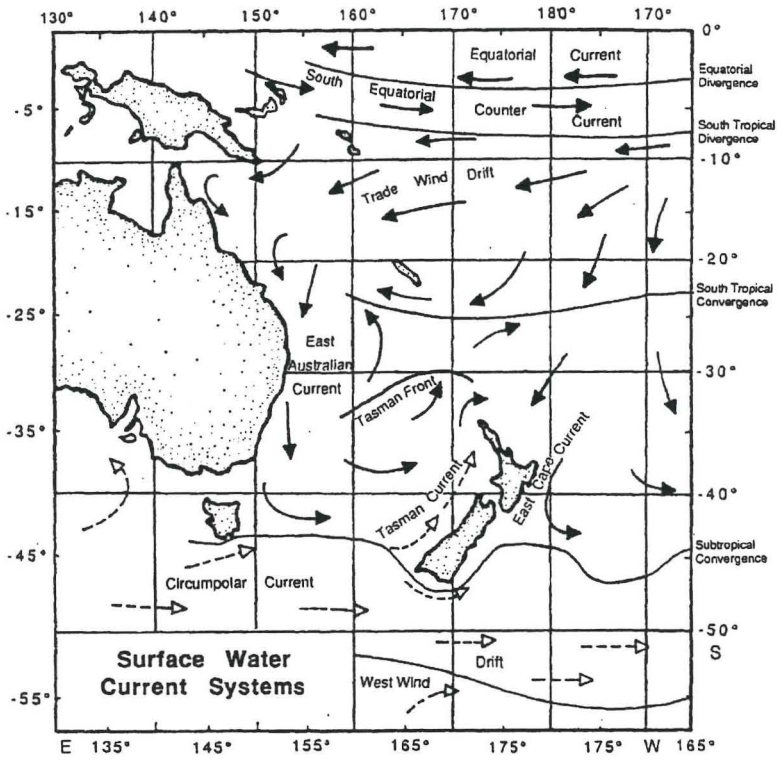

Fig.2-5: Sea surface circulation and the oceanographic front system of the Tasman Sea, SW Pacific. (After Mc Lellan, 1965; Knox, 1970; Pickard et al., 1977; Gilmour and Cole, 1979; Stanton, 1981; Stanton and Ridgway, 1988; Bradford-Grieve et al., 1991)

Water masses

Anarctic Surface Water (AASW)

In the Antarctic region the surface waters have very low temperatures (reaching a minimum of -1.9°C) and low salinity (33.5) as a result of ice melting in summer. The influence of the AASW (Antarctic Surface Water) can be traced in the upper 100-150m of the water column.

In contrast to the Antarctic Zone, surface waters in the Subantarctic region, have a larger temperature and salinity range due to seasonal changes in rainfall, insolation and evaporation.

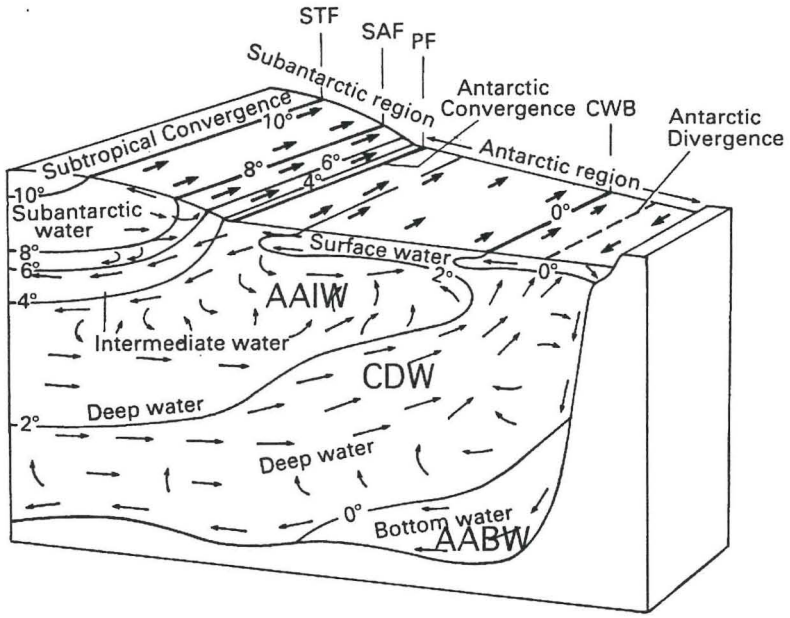

Fig.2-6: Block diagram of the water masses and circulation in the Southern Ocean, including divergences, convergences and oceanic fronts. (From Sverdrup et al., 1942)
AABW: Antarctic Bottom Water, CDW: Circumpolar Deep Water, AAIW: Antarctic Intermediate Water, STF: Subtropical Front, SAF: Subantarctic Front, PF: Polar Front, CWB: Coastal Water Boundary.

Antarctic Intermediate Water (AAIW)

The AAIW is the most extensive and important water mass at intermediate depths in the world oceans (Emery and Meinke, 1986) and is formed at about 55°-60° S, along the Antarctic Convergence (Polar Front). Due to Ekman pumping (downwelling), the AAIW is forced to sink down to approximately 500 to 1500m water depth. The AAIW is characterised by a temperature range of 2°-10°C, a salinity minimum between 33.8 - 34.5, and oxygen saturation level of up to 95%.

Since most of the AAIW is formed in the Pacific Sector of Antarctica, variations in the strength and thickness of the AAIW in this part of the ocean is thought to have played an important role in the global climate in the past (KEIR 1988).
In connection with the AAIW, Heath (1995) has indicated the presence of the Subantarctic Mode Water (SAMW) at a depth between 400 and 600 m north of the Subantarctic Front. This SAMW is a thick, well oxygenated subsurface layer which is almost isothermal (8°-10°C) and is believed to originate in the region between 43° and 48°S in the SE Pacific (Orsi et al., 1994).
Due to their similar salinity and temperature values, the relationship between the SAMW and the AAIW in the Southern Pacific is not fully understood (see discussion in Tomczak, 1994).
Wyrtki (1988) mentioned a subsurface salinity maximum extending about 80 km south of the Subtropical Convergence (STC) (information from surveys west of Australia to Antarctica, Bass Strait to Antarctica and Tasmania to Antarctica). As these surveys were made during the spring season, this salinity maximum may represent a seasonal phenomenon rather than a permanent feature.

Circumpolar Deep Water (CDW)

The Circumpolar Deep Water (CDW) underlies the AAIW and flows northward. The composition of the CDW is 45% Weddell Sea water, 30% Pacific and Indian Ocean Intermediate Water, and 25 % deep water from the North Atlantic (NADW).

Antarctic Bottom Water (AABW)

The origin of the AABW lies in vertical convection along the Antarctic continental shelf caused by the freezing of sea ice (Tomczak, 1994). The cooled water sinks to the bottom and mixes with water of the Circumpolar Current and with North Atlantic Deep Water. Most of the AABW is formed in the Weddell Sea and the Ross Sea (see fig. 2-4).
After reaching the sea floor, the AABW flows northward and extends to the Northern Hemisphere in the Atlantic and Pacific (e.g.: up to the latitude of the New Foundland Rise in the North Atlantic at ca. 40°N).

Movements of the Southern Ocean Front system during the LGM:

Subtropical Front (STF)

Howard and Prell, (1992) have deduced that apart from four brief poleward excursions, the STF was positioned equatorwards of its modern location on the Kerguelen Plateau (40°S) for most of the past 500ky. The polar front in that area was positioned near 46°S during the same time period, with brief equatorward excursions of approximately 2° latitude at ca. 120ky BP, 330ky BP and 400ky BP. During the LGM, the STF was positioned north of 42°S at 145°E and probably close to the 38°S at 140°E in the Tasmanian region. The front retreated southward to 42°S at 145°E during subsequent deglaciation. In the Holocene the southern limits established themselves south of 47°S (see fig. 2-7).

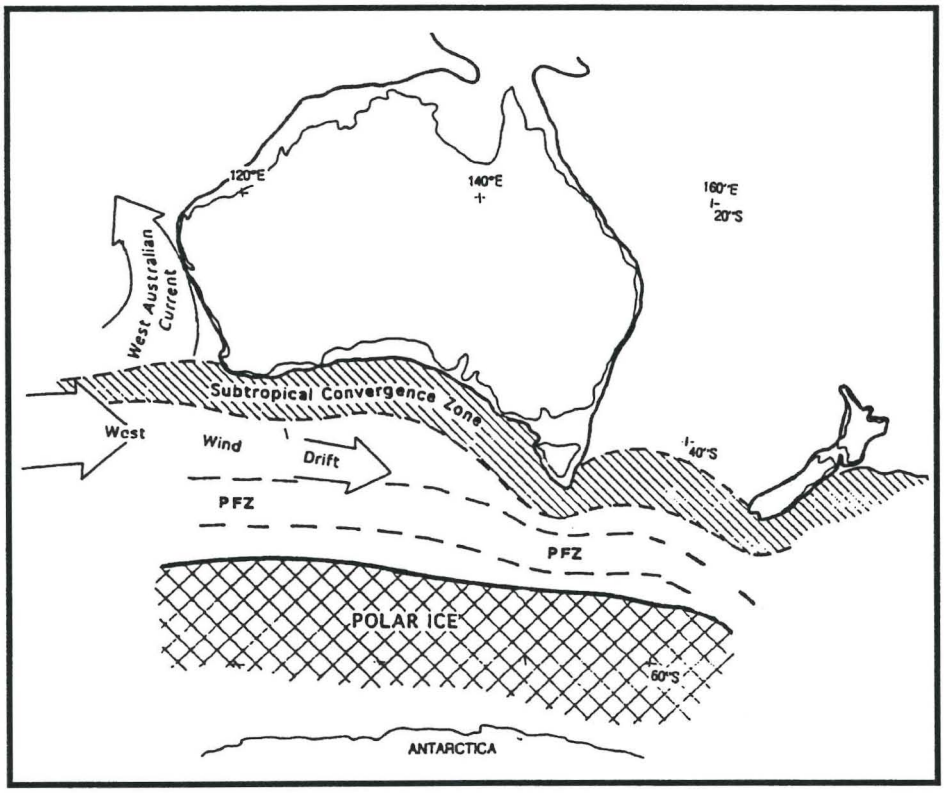

Fig.2-7: Northward shift of the Subantarctic Zone and the Polar Front Zone (PFZ) during the LGM (ca 18ky BP), after Wells and Okada (1996).

After Wells and Okada (1996), the STF was situated close to 38°S during the LGM and moved progressively southward during the following deglaciation.

Polar Front Zone (PFZ)

The movements of the Polar Front Zone were deduced by different carbonate contents and paleotemperatures of deep sea cores (Wells and Okada, 1996).

South of the STF, the carbonate content of the coarse fraction of the Polar Front Zone is close to 100%. Within the Polar Front, the carbonate content is reduced to 5 - 30% and siliceous sponge spicules and siliceous oozes make up the rest of the sand fraction. The Polar Front Zone did not extend as far north as 47° S in the vicinity of the STF during the LGM.

South of Tasmania at 145°-146°E, the Polar Front has remained south of 47°S during the last 500ky.

2.3. PLATE TECTONICS AND BATHYMETRY

Plate tectonics

During the Late Jurassic, first plate movements caused the development of a rifting zone between Antarctica and Australia, initiating the separation of both continents (AGSO Cruise 147 Report, 1995/96). This was the onset of the fragmentation of Antarctica, Australia and New Zealand that built the Gondwana remnant at these times.

Australia and Antarctica separated at the Paleocene-Eocene-Boundary (ca. 55Ma BP), allowing initial shallow water exchange between the Southern Indian Ocean and the Southern Pacific (fig. 2-8). Spreading was slow and the direction was NW for the Late Jurassic to Middle Eocene time period.

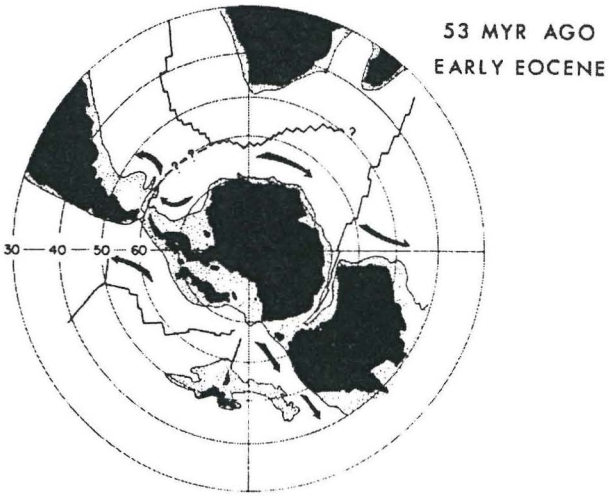

Fig.2-8: Paleogeographic position of Antarctica and Australia during the early Eocene (53Ma BP). In these times the spreading between Australia and Antarctica began and Australia moved northward. Spreading ridges and fracture zones are shown as jagged lines, black arrows indicate estimated bottom circulation. (From Kennett, 1982)

During the early Oligocene, the spreading between Antarctica and South America began. Australia continued its northward movement away from Antarctica. The spreading accelerated and changed to a N-S direction. During the early part of the late Oligocene, the South Tasman Rise was finally separated from Antarctica (see fig. 2-9). As a result of this, the Antarctic Circumpolar Current developed and cut off Antarctica from the warmer oceans in the north. Due to a decrease of meridional heat exchange, the temperature gradient between these regions increased.

Bottom water circulation was hindered by the still shallow Drake Passage and the submerging South Tasman Rise.

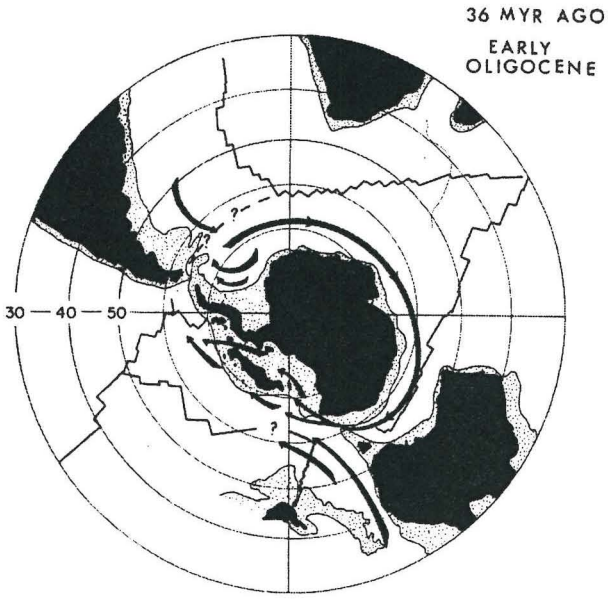

Fig.2-9: Paleogeographic position of Antarctica and Australia during the earliest Oligocene (36Ma BP). Although a substantial ocean has formed between Australia and Antarctica, deep circum-Antarctic flow still is prevented by the southernmost extension of Australia, the South Tasman Rise. The Drake Passage between South America and Antarctica remains closed. Spreading ridges and fracture zones are shown as jagged lines, black arrows indicate estimated surface water circulation. (From Kennett, 1982)

During the early Miocene, the South Tasman Rise became separated from Antarctica, allowing deep water exchange throughout all oceans (see fig. 2-10).

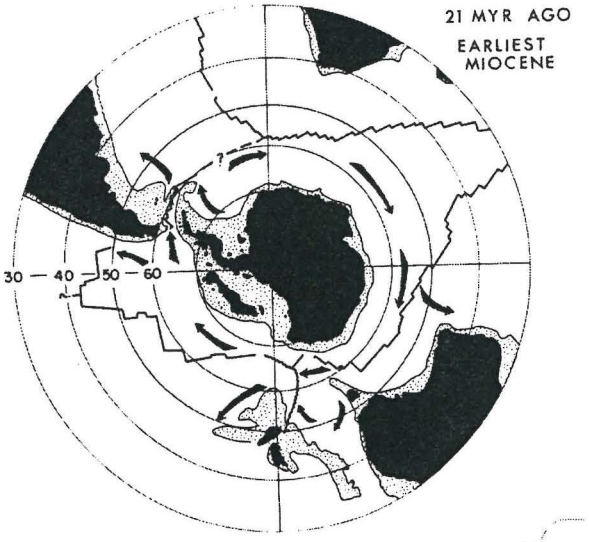

Fig.2-10: Paleogeographic position of Antarctica and Australia at the Paleogene - Neogene - Boundary (21Ma BP). Spreading ridges and fracture zones are shown as jagged lines, black arrows indicate estimated bottom circulation. (From Kennett, 1982)

The South Tasman Rise separated from Antarctica and the Drake Passage deepened, allowing bottom water transport to develop and as a result, the formation of the ACC.

By the early Miocene, the ocean basins had essentially reached their modern shapes, if not the same proportions (Kennett, 1982).

Strong katabatic winds* coming from the growing ice sheets of the Antarctica's interior, had already started the cooling of the surrounding oceans.

This and the forming of the ACC led to accelerated bottom- and deep- water formation from the Middle Miocene on. Increasing glaciation on the Antarctic continent during the Miocene, laid the foundation-stone of the Middle Miocene glaciation and the subsequently following Upper Miocene glaciation (Messinian Event). By the early Pliocene, conditions in the Southern Ocean were close to those of the Quaternary (Kennett, 1982).

The South Tasman Rise (STR)

The STR forms the southern prolongation of the Australian Continent and covers an area of 140000 km^2. This northwest-southeast trending rise, consists of continental crust (AGSO Cruise 147 Report, 1995/96) and lies approximately 800 to 3000m below sea surface. Separated from the continent of Australia by a WNW-trending, 3000m deep saddle, it is encompassed by the Southeast Indian Ocean in the west and the Tasman Basin in the east (see fig. 2-11).

The STR is the smallest fragment of the former East Gondwana continent and was bounded by Victoria Land (Antarctica) to the west, by the Ross Sea shelf to the south, by the Campbell Plateau to the south-east, by the Challenger Plateau and the Lord Howe Rise to the east and by Tasmania and Australia to the north (Exon et al., 1995/1996). Because of its central position within the East Gondwana plate

* Katabatic winds: In this case the geography is characterised by a cold plateau adjacent to a relatively warm region. Such conditions are satisfied in areas in which major ice sheets or cold, elevated land surfaces border warmer, large bodies of water. Air over the cold plateau cools and forms a large dome of cold, dense air. Unless held back by background wind conditions, this cold air will spill over into the lower elevations with speeds that vary from gentle (a few kilometres per hour) to intense (93 to 185 kilometres per hour), depending on the incline of the slope of the terrain and the distribution of the background pressure field and will cool down the adjacent water masses (ref.: http://www.eb.com:180/).

boundary framework, it underwent all the major tectonic events, that led to the splitting of the Gondwana fragments. These extensional tectonic events span from the Late Jurassic to the Late Oligocene, after which the STR drifted passively northward with the Australian plate (Exon et al., 1995). As a consequence of the changed movement directions from initially NW to N the STR shows an older NW - trending and a younger N - S - trending fault system, with the latter one having disrupted the older north-west fabric (Exon et al., 1995/1996).

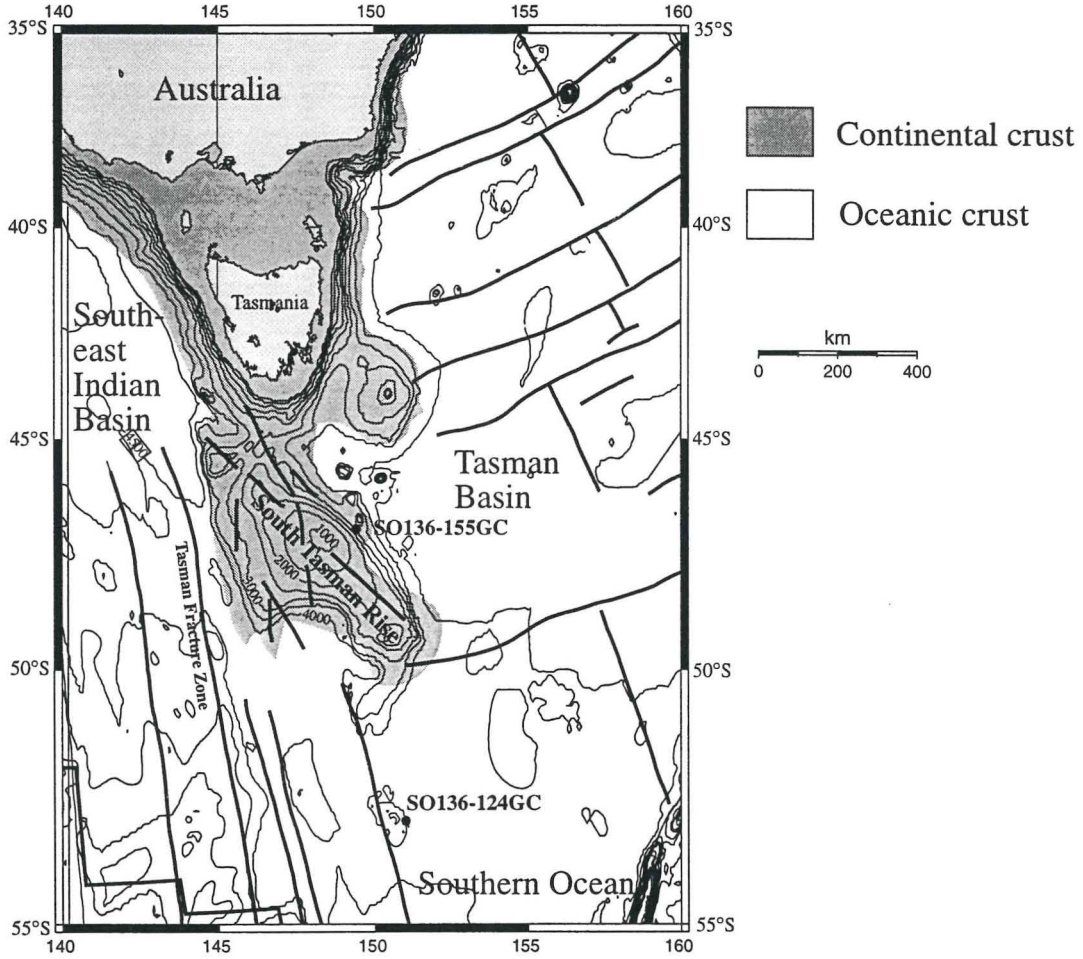

Fig. 2-11: Bathymetric map of Southern Australia and the South Tasman Rise area. Fracture Zones are shown as bold black lines. In addition, the core locations of the two studied cores are marked. Map was constructed with the "Make a Map" program (http://www.aquarius.geomar.de/omc/make_map.html).

The STR is bounded to the west by the Tasman Fracture Zone, which extends south down to Antarctica (see fig. 2-11). The Tasman Fracture Zone is a ridge about 1000m high that separates the rough sediment uncovered oceanic crust to the west from the sedimented area south of the South Tasman Rise and results from Late Cretaceous to Early Cainozoic extensional tectonism (AGSO Cruise 147 Report, 1995/96).

On November 4th 1998, a 12m gravity corer was deployed at site 23, lat.: 52°59.77 S and long.: 151°08.14 E. At 01:27 UTC. and core SO136-124GC was retrieved, the first of the two sediment cores discussed in this thesis (see figure 2-1). The water depth at this site is 4141m (cable length). The total length of the core is 7.77m. Some manganese horizons were found within the sediment column.
At 08:19 UTC, on the 8th of November, core SO136-155GC with a total length of 7.57m was taken. The exact position is lat.: 47°00.09 S, long.: 149°31.30 E (see figure 2-1). The depth at this site is between 3170m (cable length). In contrast to SO136-124GC, this core is a carbonate rich core, mainly consisting of foraminiferal sands.

Table I shows the core data of sediment cores SO136-124GC and SO136-155GC:

Core	**SO136-124GC**	**SO136-155GC**
Position	lat.: 52°59.77 S long.: 151°08.14 E	lat.: 47°00.09 S long.: 149°31.30 E
Site	23	32
Water depth (cable length)	4141m	3170
Core length	7.77m	7.57m

During the IMAGES III cruise (May 1997), the French R.V. MARION DUFRESNE took a 20.08m long sediment core at position: latitude 48°30.00S, longitude 149°06.65 E (see figure 2-1). The water depth at this position was about 2140m. This core formed the data base of a M.Sc. thesis written by Johanna Suhonen at GEOMAR in 1998. As this site is nearly in the middle of the transect between the SONNE core locations mentioned above, the results evaluated by Nees et al. (1998), might provide valuable information when interpreting sedimentary features in the investigated area.

3.1.2. Coring methods and sampling

To gather both sediment cores, a gravity corer was deployed, mounted with a lead weight of 3 tons. Two main steel tubes, each 5.75m in length, were combined into one coring tube. The inner plastic liners, containing the sediment, are 12.5 cm in

diameter with a wall thickness of 0.25 cm. A core catcher was used to prevent sediment loss when pulling the coring device out of the sediment.

The gravity corer was lowered with an average speed of 1.5 m/s. To prevent non-perpendicular penetration of the corer due to swinging, a short stop was arranged at about 200m above sediment surface. After penetrating the seabed (at ca. 1.5 m/s) it was pulled up with a speed of ca. 1 m/s.

After surfacing, the core was brought on the deck, cut into 1m sections and was stored inside the logging container for a minimum time span of 2-3 hours, to acclimatize. Acclimatization was done to minimize the effect of temperature dependent density changes during the Multi Sensor Track (MST) - Logging process.

The logging measurements were made with a track-mounted GEOTEK Multisensor Core Logger (for details see section 3.1.4).

After the logging, the 1m core-sections were split and carried into the sedimentary laboratory where the archive halves were packed and stored in the cold storage room.

The working half was described sedimentologically and then logged with a Minolta Camera (CM 2002) to get the colourimetrical data. After this procedure was completed the core was sampled every five cm using syringes. Finally, the working half was also packed into so-called D-tubes and stored in the cooling room.

3.1.3. Visual core description

After splitting into two halves, the 1m core sections were described visually. To achieve a uniform description mode, all core descriptions were done by the supervisor of the sedimentary laboratory. The ODP (Ocean Drilling Program) visual core description forms were used to systematically describe the lithology, the grain sizes, sedimentary structures and visual colour determination (via Munsell Colour Chart). Afterwards, the core descriptions were digitized.

3.1.4. $CaCO_3$ - analysis

Following the visual core description, the working halves were sampled in 25 cm intervals, to carry out the $CaCO_3$ analysis, using the so-called *carbonate bomb* technique (Cruise Report SO136, 1999). The instrument was standardised by pure $CaCO_3$. It measures the CO_2 pressure release following the reaction of HCL with calcium carbonate. The amount of sediment taken for the measurements was standardised to 0.75 g. Weighing on board was hampered by heavy swell and therefore might include some errors. The measurement of calcium carbonate concentration lower than 5 % is not possible using the *carbonate bomb* method(Cruise Report SO136, 1999).

3.1.5. Colour determination (Spectrophotometry)

A spectral photometer (Minolta CM 2002) was deployed, to achieve optical data of the sediment in the wavelength range of 400 nm to 700 nm (visible light). Directly after the visual core description, the working halves of the taken cores were analysed. To protect the camera from being polluted by sediment, the core halves were covered by transparent plastic foil, which made sampling in the SCE-Mode (Specular Component Excluded) necessary. The measurement area of the spectrophotometer is 8 mm. To achieve the highest possible resolution, a sampling interval of 1 cm was chosen throughout all analysed cores. The Minolta was calibrated with black and a white standard before every new core measurement, occasionally in between the sections, whenever the time-distances extended to more than an hour.

Measuring principle

The CM 2002 is equipped with a pulsed xenon arc lamp which illuminates the integrating sphere of the spectrophotometer. Diffusely backscattered, the light hits the target, becomes reflected and is focused on a silicon photodiode. The reflectance-intensity of a wavelength range of 400 nm - 700 nm (in 10 nm pitches), L*, a*, b* values and data of the Munsell Colour System are detected by this sensor. The camera was connected on-line to a Macintosh LC computer where the

data were stored and subsequently analysed. The CM 2002 inserted several zero-measurements throughout the cores. In order to get the correct values for the distinct core-depths, these zero-measurements had to be removed before plotting the data.

3.1.6. Multi Sensor Track (MST)

A track mounted GEOTEK MSCL Multisensor Core Logger was used, to measure the physical properties of the sediments on board. This Multi Sensor Track (MST) includes the following sensors:

1. Gamma-ray attenuation porosity evaluator (GRAPE) for wet bulk density estimates;
2. P-wave logger (PWL) for acoustic velocity estimates, including a sensor for the core diameter measurements;
3. Bartington Instrument loop sensor for measurements of the magnetic susceptibility (MS).

At the beginning of each core MST run, the system was calibrated by a 20cm calibration section.

The unsplit 1m sections of all cores were passed through this MST-Logger on a motor driven conveyor belt. Measurements were taken at 2 cm intervals.

The data were processed with the GEOTEK software, which ran under the Microsoft Windows operating system.

3.1.6.1. The GRAPE system

The GRAPE operating system consists of a gamma ray source and a detector mounted opposite each other at the level of the core centre. A 10 milli-curie Caesium-137 capsule was used as the gamma ray source. The emitted photons pass through the core and become partially scattered. The unscattered gamma photons are detected on the other side. By measuring the number of unscattered gamma photons that pass through the core the density of the sediment can be determined (GEOTEK MSCL Manual, 1998).

3.1.6.2. The P - wave Logger

An Ultrasonic P-wave system was used to measure the P wave velocity through the core. It uses two piston-type 500 kHz transducers. To maintain a continuous acoustic coupling between the transducer faces and the core liner, water was sprayed on the liner. For the measurements a short P-wave pulse is produced at the transmitter. This pulse propagates through the core and is detected by a receiver. Pulse time circuity is used to measure the travel time of the pulse. The distance travelled is measured as the outside diameter of the core with an accuracy of 0.1mm. After suitable calibrations, the p-wave velocity can be calculated with a resolution of ca. 1.5 m/s. Although the accuracy of the measurements depends on any variations of the liner wall thickness, an absolute accuracy of ± 3 m/s is achievable (GEOTEK MSCL Manual, 1998). As the end caps were left taped to the core sections, approximately 4-6 cm of the P-wave measurements at each section ends are of poor quality and therefore were rejected. The thickness or diameter of the core is measured as the distance between the active faces of the two transducers. Therefore an additional displacement transducer was coupled to the P-wave transducers. These displacement transducers follow the movements of the P-wave transducers and the core diameter is calculated from the deviation of the preadjusted reference thickness.

3.1.6.3. The magnetic susceptibility (MS) measurements

A Bartington Instrument loop sensor (MS2C) with a inner diameter of 16 cm was used for measurements of the magnetic susceptibility (MS). The measurement of MS therefore provides information about the amount of magnetic responding material inside the sediment. An oscillator circuit in the sensor produces a low intensity (approximately 80 A/m) non saturating alternating magnetic field. The electronics convert this pulsed frequency into magnetic susceptibility values. Errors may occur due to any material in the vicinity of the sensor that has a magnetic susceptibility which might cause a change in the oscillator frequency (GEOTEK MSCL Manual, 1998). Half an hour before logging, the sensor was switched on to allow equilibration. The sensor was zeroed before each core logging process. The MS data of core SO136-124GC are raw values in SI units, the data of core SO136-155GC had to be corrected, due to instrument drift.

3.2. LABORATORY METHODS

Both sediment cores, SO136-124GC and SO136-155GC, were sampled at 5 cm intervals down to a depth of 5m. All in all 200 samples were taken and analysed. The sequence of the laboratory methods is shown in figure 3-2.

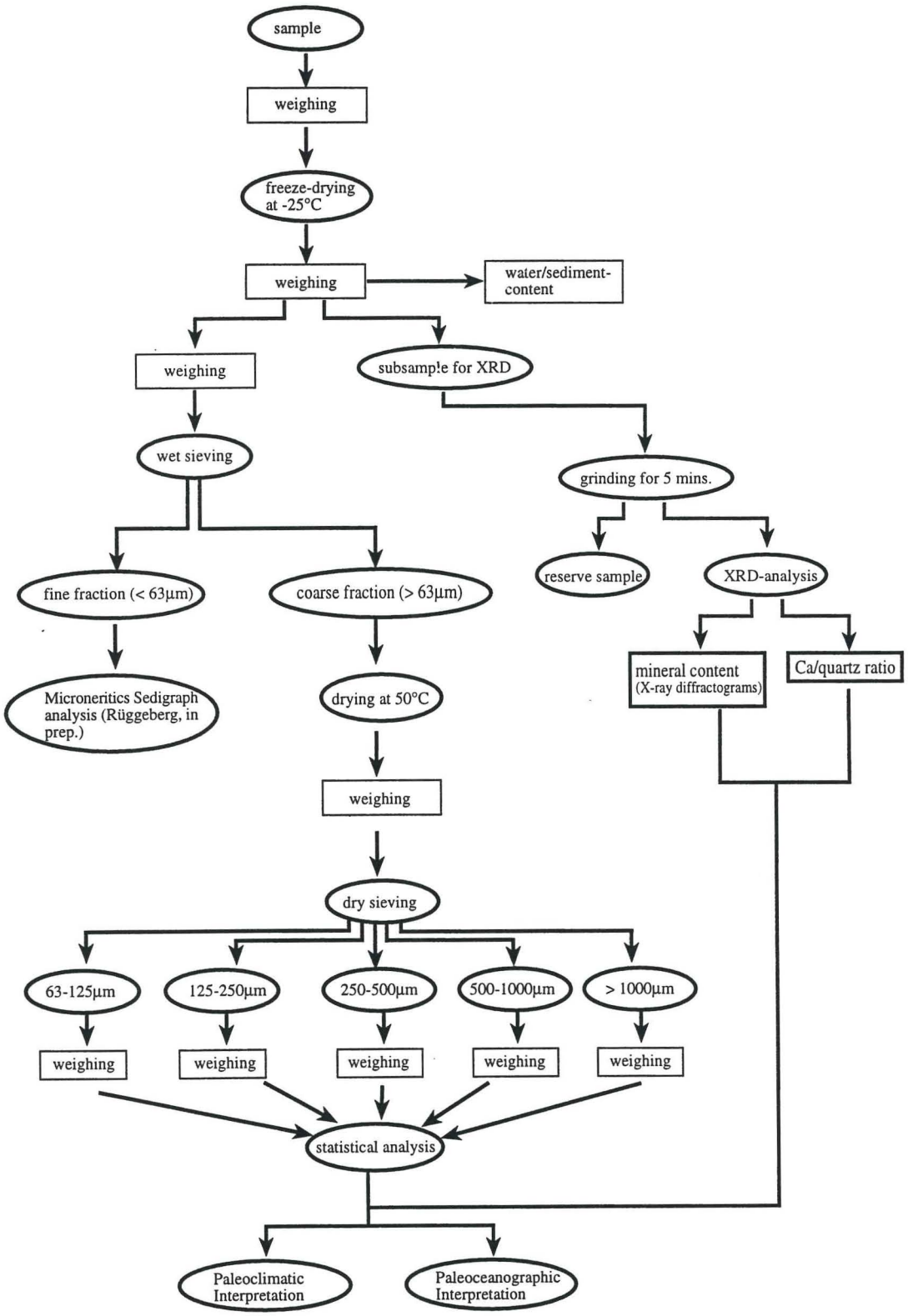

Fig. 3-2: Sketch of the applied laboratory techniques.

3.2.1. Physical properties

After sampling, weighing and freeze drying, the samples were weighed again, to obtain the water content of the sediment or the sediment content of the sample, respectively (see fig. 3-2).
Information about the sediment - water ratio of the samples may provide a first idea of the sediments nature (density and water content).

3.2.2. X-ray diffraction (XRD)

The XRD analysis was used to study the mineralogy of the sediments. To obtain an overview of the mineral contents, analysis of the whole rock samples (bulk sediment) was performed.

To get satisfactory results, the grain size of the sediment had to be reduced to 5 - 10 µm. Therefore the samples were carefully ground for a minimum time span of five minutes in an agate mortar. The grinding was done by hand to achieve the most possible homogeneity. In case of the presence of some larger quartz grains in single samples, these grains were ground again until a satisfactory homogenous material was achieved.

After grinding, the samples were filled in a cavity mount holder made of aluminium. The samples were filled in with as little pressure as possible, to produce a random sample. Thirty-five of these filled aluminium holders were packed into a magazine and measured in one run.
The analysis was carried out using a Philips PW 1700 X-ray diffractometer containing a cobalt anode.

The samples of core SO136-155GC were scanned from 25° - 40° (2Θ -values), to focus the studies on the main peaks of the carbonate minerals like aragonite and calcite. While sediment core SO136-124GC showed more terrigenous components, the scanning range was extended to 0° - 40° (2Θ -values) to detect the peaks of the clay minerals.
All samples were scanned with a speed of 0.01 per second at 40 kV and 35 mA.

The generated X-ray diffraction PC files were analysed using the MacDiff 4.0.3 software for Macintosh computers developed by Petschik (1999).

The first aim was to get a qualitative overview of the mineral content of both sediment cores. Afterwards, the $CaCO_3$ to Quartz ratios were quantitatively analysed to obtain a signal of glacial/interglacial changes.

Another objective was to check the possible presence of high-magnesium calcite (HMC) as input from the STR.

3.2.3. Grain size distribution

After freeze drying (at -25°C) and weighing, the samples were wet sieved with a 63 µm sieve to separate the coarse fraction (> 63µm) and the fine fraction (< 63µm). The fine fraction was collected in a 5 litre jar for further grain size analysis using a Microneritics Sedigraph (Rüggeberg, in prep.). Because of the amount of fine fraction (<63µm) of the samples of sediment core SO136-124GC, two of these 5 litre jars had to be used.

The samples were dried again at 50° C, the coarse fraction was dry sieved and divided into five subfractions (63-125µm, 125-250µm, 250-500µm, 500-1000µm and >1000µm), to achieve the grain size distribution of the coarse fractions (see fig. 3-1). These subfractions were weighed again and statistically analysed.

Afterwards, the subfractions 63-125µm, 125-250µm and 250-500µm were biostratigraphically investigated by Rüggeberg (in prep.).

4. RESULTS

4.1. Lithology

SO136-124GC (fig. 4-1)

The sediments throughout the core are of silty to clayey nature. Radiolarian-bearing to radiolarian-rich silicious clays make up the main part of the sediments. Three sections are burrowed more intense. (0-25cm, 235-375cm and 475cm downcore). The rest of the core showed little to rare bioturbation. Manganese grains are present as well and in total 4 manganese horizons were discovered.

The upper section (0 - 8cm) of this core is covered by a well sorted manganese pavement. The size of the manganese nodules at the core top varies between 3 - 5cm in diameter. Subrounded quartz grains build the matrix of these manganese nodules.

The core section from 8 - 96cm shows a coarsening upwards cycle with soft calcareous foram-bearing silty clay at the top and a manganese-rich siliceous clay at the base. From 32 to 36cm within this section, another manganese horizon was found. With 6 - 8cm in diameter, the size of these nodules is slightly larger than the size of those at surface. The sediment colours in this section vary from very pale brown at the top to dark brown at the base.

Very fine sandy to fine sandy, radiolarian-, manganese- and quartz -bearing firm to stiff clay makes up the sediment in the core section from 96 - 196cm. It also contains some granular and pebble sized manganese nodules. The colour is dark brown.

From 196 to 275cm a second coarsening upwards cycle was detected, from fine sand at the top to very fine sand at the base. The colours vary from light yellowish brown to grayish brown and pale brown.

Sediments of very pale brown to pale brown colour dominate in the core section from 275 - 375cm. These sediments are built by a very firm, Mn-rich, radiolarian- and quartz-bearing clay. The quartz grains (very fine sand) are well sorted.
A buried manganese horizon was found in the core section between 362 and 369cm. The nodules are 6 - 8cm in diameter and are strongly corroded.

Manganese-rich, radiolarian- and quartz-bearing clays make up the rest of the core (375 - 773cm). The radiolarians and the quartz grains represent the coarse silt fraction in a clayey matrix. Colours vary from pale brown, pale yellow, light olive brown to dark brown with the lighter units containing more radiolarians and

SO-136-155GC (fig. 4-2)

Sediment core SO-136-155GC was recovered from the north-eastern flank of the South Tasman Rise at a water depth of 3170 (for details see fig. 3-1, page 21). The sediments of this core are carbonate rich and are mainly made up of coarse sand- to silt- sized foraminiferal sands and foram marl oozes. Bioturbation is rare.

The upper 300cm of the core are characterized by undisturbed sedimentation. Below this level, three fining upwards cycles mark the occurrence of turbidite sequences, which make up the rest of the core.

The upper core section (0 to 91cm) consists of fine sand sized foram-bearing marl ooze with a grayish to yellowish colour, that grades into a medium sized foram-bearing marl ooze (91 - 100cm).

Downcore, 100 - 254cm, a sequence of varying, fine sand to medium sand sized foram ooze occurs. The colour is white to grayish with pale green laminations and reddish gray streaks (diagenetic horizons) consisting of pyrite, glauconite and manganese. Due to bioturbation, the colour boundaries are slightly blurred.

Core section 254 - 304cm is characterized by foram marl ooze to foram sand of grayish colour with pale green, pale red and pale yellow streaks.

A fining upwards cycle (between 304 - 342cm) with very fine sandy to silty foram sand on top and fine sand sized foram sand (phreatic horizon) at the bottom marks the upper level of a series of turbidites.

A second turbidite at depth between 374 and 562cm is marked by a fining upwards cycle from very fine sand, over fine sand to medium sand. Within this unit foraminifera, needles and spines are present, as well as black angular grains.

At 562cm an erosive boundary was discovered, below which (562 - 681cm) another turbidite is indicated by another fining upwards sequence.

The bottom of the core (681 - 756cm) is made up of foram marl ooze. The purple and greenish streaks mentioned above persist throughout the entire core (for details see fig. 4-2).

SO136-124-GC (fig. 4-3)

In sediment core SO136-124-GC, $CaCO_3$ values range from 0 to 58%.

With 58%, the Holocene (0 - 22cm) shows the highest values within the entire core. $CaCO_3$ contents of 0 to 10% in the core section from 22 - 185cm characterize oxygen isotopic stages 2 - 4, whereas the short increase to higher values (~10%) around 100cm might represent isotope stage 3.

Isotope stage 5 (185 - 285cm) again shows comparably higher carbonate values about 30% indicating a warmer period of increased carbonate production.

After a sharp drop to almost 0% $CaCO_3$ during stage 6, a remarkable increase of values indicate stage 7 (318 - 365cm).

Below stage 7 (from 365cm downcore) the $CaCO_3$ contents converge versus zero to remain very low for the rest of the core.

SO136-155-GC (fig 4-3)

Throughout core SO136-155-GC, values of the $CaCO_3$ contents are very high (from 81 - 91%).

Like in core SO136-124-GC, the Holocene (0 - 25cm) shows the highest values (91%).

A drop in values to ~85% between 25 and 130cm in core represents oxygen isotopic stages 2 to 4. Between 80 and 105cm, a short peak of $CaCO_3$ values to approximately 87% might represent isotope stage 3.

After an increase to 86 - 90% during stage 5 (between 130 and 260cm below core top), the values decrease at the transition from stage 5 to stage 6 (~260cm) to values of around 82 - 83%.

As the rest of the core is made up by a series of turbidites, the fluctuations of the $CaCO_3$ values from approximately 290cm downward are steered by the mechanisms of gravity flows.

SO136-124GC (fig. 4-4):

All spectrophotometrical data (L*-values, a*-values, b*-values and the spectrum 400-700nm) show similar features. The graphs clearly show the glacial (low values) and interglacial (high values) time periods. Whereas L*-values and 700nm-values show better resolution for interglacial stages, glacial periods are better characterized by the b*-values.

Throughout the core, L*-values of core SO136-124GC range between 42 and 61 (dimensionless values, from 0 to 100). Interglacial periods (9, 7, 5 and Holocene) show values between 50 and 62, with the highest values at the end of stage 9 and during the Eemian.

L*-values for the glacial periods are clearly lower, with the lowest point during stage 2, whereas the highest values do not exceed 56.

However, the resolution during stages 2 - 4 is not as good as during the other stages.

SO136-155GC (fig. 4-5):

For core SO136-155GC the L*-values (black line), the 550nm- (green line) and the 700nm curve (red line) are plotted. Qualitatively, the graphs show similar features like those for core SO136-124GC: higher values during interglacial stages, lower values in glacial periods.

The L*-values are between 65 and 83 (dimensionless from 0 - 100) throughout the core. Stage 5e shows the highest values (~ 83), lowest values are reached during stage 6 (~ 65) and the Last Glacial Maximum (~ 66). Whether the negative peak during stage 6 still belongs to the part of undisturbed sedimentation is questionable. This feature is possibly an imprint of the turbidite, following stage 6 downcore.

The positive peak below stage 6 is not a time signal, but a sedimentological feature. The undisturbed sedimentation ends during stage 6 below which turbidite sedimentation prevails for the rest of the core (see fig. 4-5).

4.4. MULTI SENSOR TRACK

4.4.1. Sediment density (the GRAPE system)

The Sediment density can be determined by measurements of the GRAPE system,. Other physical properties like porosity, water content and dry density can be mathematically deduced by the GRAPE measurements (Jian Chi, 1995).

Generally, the knowledge of the sediment density alone does not provide enough information to interpret glacial and interglacial cycles or sedimentological features. If the sediment is not homogeneous, like in core SO136-124GC, the density of the single mineral grains had to be known and the grains had to be investigated quantitatively.

However, if the sediment is uniform, like in sediment core SO136-155GC, a direct link from density to grain size distribution can be made.

The gaps in the graphs correspond to the section breaks. During the measurements the end caps were left taped to the section ends. At these positions the density measurements showed lower values which had to be rejected.

SO136-124GC (fig. 4-6)

Density variations for this core range from 1.4 to 1.8g/cm^3. As this sediment core is dominated by terrigenous material, especially during the glacial periods, it is very heterogeneous and no clear interpretation can be made by the density signal, only. However, if averaged, the values corresponding to interglacial periods are slightly higher than those for glacial times.

During the Holocene (0 - 22cm), a major peak in high density values (~1.8g/cm^3) occurs at about 10 - 15cm core depth.

During oxygen isotopic stages 2 to 4 (22 - 186cm) density values are generally low, 1.4 to 1.55g/cm^3. An exception is the double peak at about 35 to 45 cm. These peaks may result from two melting phases at the end of the LGM.

The high values (1.53 - 1.62g/cm^3) during oxygen isotopic stage 5 (186 - 282cm) diminish slightly at the transition from oxygen isotopic stage 5 to stage 6 (282 - 318cm) to values around 1.52g/cm^3.

Isotope stage 7 (318 - 357cm) shows even higher values than stage 5 (1.55 to 1.65 g/cm^3).

Below stage 7 (357 - 500cm) lower values (1.6 - 1.45g/cm^3) occur, possibly indicating another glacial period. The high density peak at 385cm is another sedimentological feature, which will be discussed later (chapter 4.5. GRAIN SIZE DISTRIBUTION). This sample consists of detritus of former carbonate crusts only, and therefore is dominated by the coarse fraction > 500µm.

SO136-155GC (fig. 4-6)

The uniformity of the sediments allows a more precise interpretation of the density values in respect to glacial and interglacial periods. High density values correspond to finer grain sizes, lower densities to coarser grain sizes, respectively. The density in core SO136-155GC varies from 1.6 to >1.8g/cm^3.

During the Holocene (0 - 25cm), the density values range from 1.74 to 1.78g/cm^3. In the core section from 25cm to 80cm, the density drops to values around 1.7 g/cm^3.

From 80cm to 105cm, higher density values (~1.77g/cm^3) might indicate higher productivity during oxygen isotope stage 3. The subsequent drop in density (<1.7g/cm^3) below that point (105 - 130cm) could correspond to times with lower temperatures during stage 4.

The sediments of isotopic stage 5 (130 - 260cm) are characterized by density values of 1.72 to >1.877g/cm^3.

The last trend detectable in this core is the transition from stage 5 to stage 6 at depth of about 260cm. At this point the density drops significantly to values below 1.7g/cm^3.

Below this point, the rest of the core investigated (500cm) is made up by two turbidite sequences.

4.4.2. P-wave velocity (fig. 22)

P-wave velocities are an indicator for sediment compactness, whereas compactness mainly depends on grain size, grain mineralogy and the consistency of the matrix as well as the grade of diagenesis.

Due to unknown reasons, p-wave logging of both sediment cores are of minor quality.

Again, gaps in the record correspond to the section ends.

SO136-124GC (see fig. 4-7)

Sediment core SO136-124-GC shows p-wave velocities around 1450m/s without any major changes. The remarkable triple peak to values less than 1200m/s in the core section from 50 to 90cm does not correspond to any of the other analysis. Major changes in p-wave velocity only occur at the section ends. Due to this observation in contrast to the weak fluctuations throughout the rest of the core, the reliability of these features is questionable.

SO136-155GC (see fig. 4-7)

This sediment core shows a narrower range of p-wave velocities from 1420m/s to <1500m/s. Although the graph shows quick fluctuations of minor changes, the average position of the p-wave values remains relatively stable at about 1445m/s throughout the core. No systematic changes correlating to glacial and interglacial changes, paleoproductivity, or sedimentology can be deduced from the p-wave curve (see fig. 4-7).

4.4.3. Magnetic susceptibility (MS)

The operating principle of MS measurements is the ability of an applied magnetic field to react on ferromagnetic minerals. These minerals are mainly Fe - oxides (magnetite, hematite) or Fe - sulphides (Rey, 1991). When interpreting the MS logs, it has to be taken into account that magnetite, with hematite the most important ferromagnetic mineral, not necessarily is of terrigenous origin but also can be biogenic. The magnetic susceptibility changes with the amount, the size and the nature of these ferromagnetic minerals.

Generally, MS - data within glacial periods show higher values. An increased input of terrigeneous material through aeolian and subaquatic processes (e.g. turbidity currents) is assumed.

During interglacial periods MS values are lower because of dilution of the terrigenous input by biogenic carbonate and silica resulting from increased bioproductivity.

SO136-124GC (fig. 4-8)

After low values of 8 - 10 SI during the Holocene (0 - 22cm), a significant increase (up to 18 SI) occurs in the core section from 22 - 45 cm. This increase might represent the LGM - time interval.

From 45 - 105 cm the MS lowers down to approx. 12 - 10 SI which could correspond to higher bioproduction during oxygen isotope stage 3.

In the core section from 105cm to 280cm, the MS values remain relatively stable around 12 SI with a slight drop to 10.5 SI at the end of this section (stage 5).

The increase to nearly 16 SI between 280cm and 320cm corresponds to oxygen isotope stage 6.

From 320cm to 380cm the MS shows values less than 12 SI, indicating another period of higher productivity (possibly stage 7).

A significant increase in MS values, up to 18 SI, at about 400cm and a drop to about 13 SI at 475cm might represent oxygen isotope stages 8 and 9.

SO136-155GC (fig. 4-8)

SO136-155-GC shows useful values from 0cm to 290cm downcore. Below that point, a series of turbidites make up the rest of the core (see chapter 4.1. LITHOLOGY). The low values between 2 SI and 4 SI are due to a very high carbonate content throughout the core.

The Holocene is characterized by very low values of about 2 - 3 SI, indicating a period of high dilution of the terrigenous material by biogenic input. The increase in the MS values at the transition from Holocene to isotope stage 2 might be the response to a melting phase after the LGM. The negative peaks within the core section from 80cm to 105cm (oxygen isotope stage 3) show the lowest values detectable within the entire core. This possibly indicates quick changes of productivity and terrigenous input in response to climatic changes. Stage 4 again shows high values about 4 SI.

During stage 5 (~ 115 - 255cm) MS values remain relatively low (about 2.5 to 3 SI) and below 260cm, an increase (> 5 SI) of the MS marks the transition from stage 5 to stage 6 which is cut off by the upper turbidite at depth about 290cm.

4.5. PHYSICAL PROPERTIES AND GRAIN SIZE DISTRIBUTION

WATER CONTENT AND %-COARSE FRACTION

The amount of coarse fraction and water content shows different tendencies for both sediment cores.

SO136-124GC (fig. 4-9):

For sediment core SO136-124GC no clear structures of the amount of coarse fraction and water content can be observed. Generally, values of water content are higher during warmer, interglacial periods and lower during colder, glacial periods, respectively.

The amount of the coarse fraction subsequently lowers downcore, from more than 60% at core top to less than 10% at the base (see fig. 4-9).

SO136-155GC (fig. 4-9):

Like in core SO136-124GC, the water content of core SO136-155GC does not show any clear structures, but fluctuates between 45% to 80% throughout the entire core.

Coarse fraction values show a clear tendency in the upper core section of undisturbed sedimentation (0-285cm). The amount of the coarse fraction increases during cold periods and decreases during warm periods. Therefore, values for the Holocene and oxygen isotope stage 5 (in the range of 30 to 40%) are relatively low, whereas the coarse fraction during stages 2-4 shows higher values (40 to 60%).

At ~300cm, a sharp drop in values of the fraction >63µm marks a mudlayer, which was sedimented on top of the upper turbidite cycle. Below that point, the coarse fraction increases and remains stable around 60 to 70% for the rest of the core.

The water content and the weight % of the coarse fraction of both sediment cores are shown in figure 4-9.

GRAIN SIZE DISTRIBUTION

The result of the grain size analysis for the two sediment cores differs significantly. Whereas core SO-136-155GC shows a bioproduction dependent signal (especially in the fraction 63 - 125µm), the grain size distribution in core SO136-124GC must be controlled by oceanographic factors like bottom currents and other depositional processes.

SO136-124GC (fig. 4-10)

During the Holocene (0-22cm) high percentages of the finer subfractions (63-125µm and 125-250µm) can be observed. They decrease downcore at the transition from oxygen isotope stage 1 to stage 2. Values of the coarser subfractions 250-500µm, 500-1000µm and >1000µm increase at this transition phase, the latter two due to ice rafted detritus (IRD). The dropstones consist of quartz, feldspars, up to 6mm in diameter which are partly manganese coated.

During stages 2 to 4 (22 - 190cm) the subfractions 63 - 125µm and 125 - 250µm slowly increase to values of 30 to 40%, whereas the coarser fractions > 250µm decrease.

Weight percentages of the fraction 63-125µm during interglacial stages 5, 7, and 9 show slightly higher values than those of glacial stages 6, 8 and 10, with the highest value of nearly 50% during stage 7. The signals of the subfractions 125-250µm and 250-500µm show no clear amplitudes.

The subfractions 500-1000µm and especially the coarsest grain size (> 1000µm) show some interesting features and therefore were investigated more in detail. The peak distribution of these fractions are steered by the input of ice rafted detritus (IRD) and by periodical occurrence of carbonate detritus. The samples with IRD mainly consist of quartz and feldspar grains, with manganese coatings.

The fragments of carbonate crusts are 3-5mm in diameter and are altered. They occur periodically at the end of the interglacial stages, at the beginning of the glacials or at the transition phases between interglacial and glacial stages (see marked peaks of the > 1000µm fraction in fig. 4-10). The formation and the origin of these carbonate fragments is discussed in chapter 5 (DISCUSSION).

Figure 4-10 shows the grain size distribution of sediment core SO136-124GC.

SO136-155GC (fig. 4-11)

The grain size distribution in this core clearly shows a signal that depends on carbonate production. The subfractions 63-125µm and 250-500µm obviously are the most foraminifera-sensitive grain sizes. Therefore their signals can be interpreted in terms of increased and decreased carbonate production and can be divided into cold and warm periods. The subfractions coarser than 500µm show values less than 1% throughout the entire core and therefore can be neglected.

Both subfractions (500-1000µm and >1000µm) are made up of foraminifera (*Globigerina truncatulinoides* sp, *Orbulina* sp.sp., *Pyrgo* sp. sp., *G. menardii* sp.), some benthic foraminifera (*Eggerella bradyi*), some big radiolarians, siliceous debris (spines and diatoms) and a few pink quartz grains.

As the subfraction 250-500µm shows the same features as the 63-125µm subfraction, but inversely correlated, it is discussed under 63-125µm.

The subfraction 125-250µm does not show any major fluctuations within the upper core section from 0-290cm. Below that point the values drop down to about 10% reflecting the occurrence of a foram ooze layer on top of the upper turbidite at depth of 290-310cm. In the core section from 310-495cm, two cycles of increased values up to more than 60% characterize the fining upward sequences of the two turbidites.

The values of the subfraction 63-125µm range from 22% to more than 80% with lower values during cold periods (glacials) and higher values during interglacials and within the foram ooze layer (see fig 4-11). This fraction shows values between 42% and 53% during the Holocene, which drop significantly to less than 25% during oxygen isotope stage 2 (25-75cm).

Stage 4 (100-130cm) is characterized by low values of around 25%, that once again increase at the transition to stage 5.

The substages of stage 5 (130-260cm) show good resolution. In this core section lowest values (~25%) occur during substage 5.1 while the highest values (~55%) are found for the Eemian period.

Below stage 5, a decrease to values of about 25% indicate oxygen isotopic stage 6 which is interrupted by the foram ooze layer on top of the upper turbidite (295-315cm). In this section the values increase to more than 80% weight.

Two fining upward cycles make up the rest of the core. In the core section from 315 to 370 (turbidite II, see fig. 4-11), values drop from 80% to ~25% and increase

Two subfractions, the finest coarse fraction (63 - 125µm) and the fraction 250 - 500µm, provide additional information and therefore are investigated more in detail. They show a good negative correlation (see fig. 4-12). The correlation coefficient R is -0.971. These two fractions obviously are the most foraminifera-sensitive grain sizes. Whereas the 63 - 125µm-fraction dominates during the warmer periods (e.g.: oxygen isotopic stages 5.5, 5.3, 5.1, 3 & 1), the coarser fraction shows higher values during the colder phases like interstadial 5.4, 5.2 as well as during glacial periods stage 2 and stage 4 (see fig. 4-11).

A necessary condition is the homogeneity of the sediment, only consisting of foraminiferal sands and oozes. Figure 4-12 shows the correlation of the two subfractions 63 - 125µm and 250 - 500µm for the core section of undisturbed sedimentation (0 - 285cm).

However, which species mainly contribute to this relation is not fully understood yet.

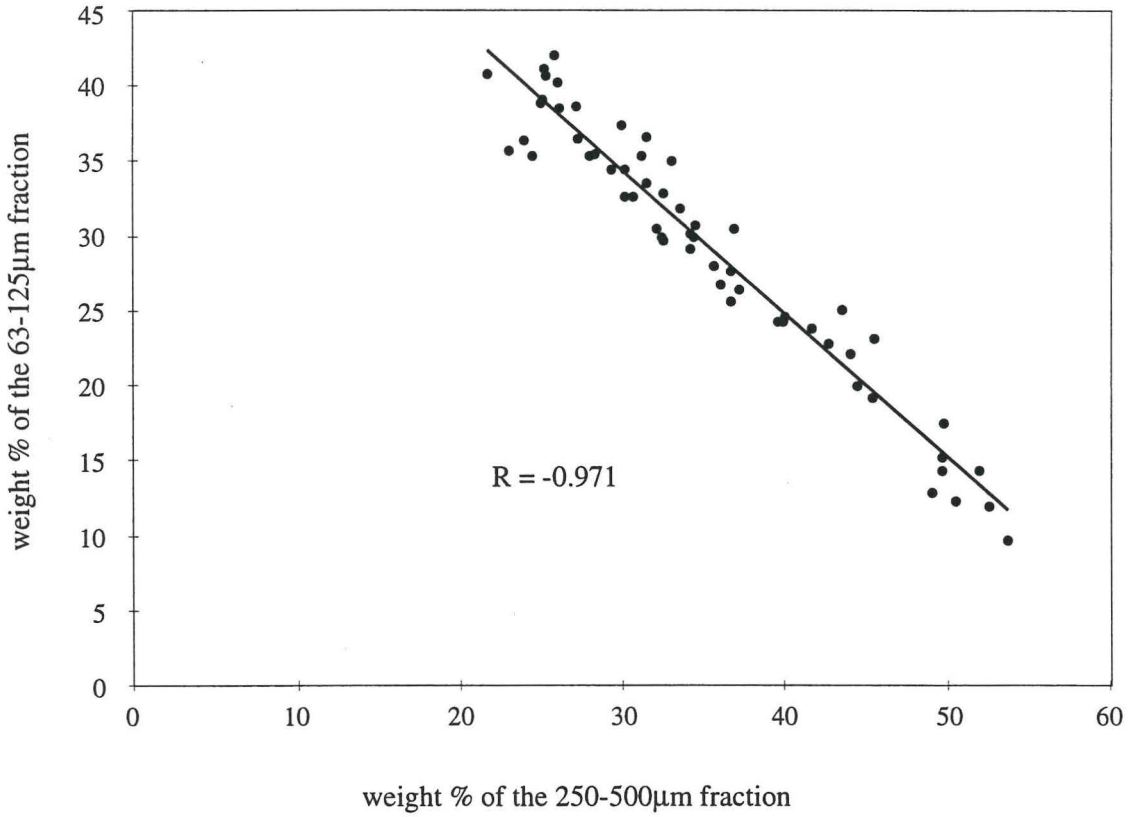

Fig. 4-12: Linear regression of the two subfractions 63-125µm and 250-500µm between core depth of 0 to 285cm (undisturbed sedimentation). The correlation coefficient R is -0.971. Below 285cm, the rest of the core is made up by turbidite sequences and therefore the relation is not valid.

Apart from quartz and calcite, feldspars like albite and orthoclase could be identified, as well as the clay mineral muscovite. The amount of these terrigenic components remains stable throughout the entire core.

The peak intensities of quartz and LMC were extracted out of the diffractograms and standardized to establish a LMC/quartz ratio curve (fig. 4-14).

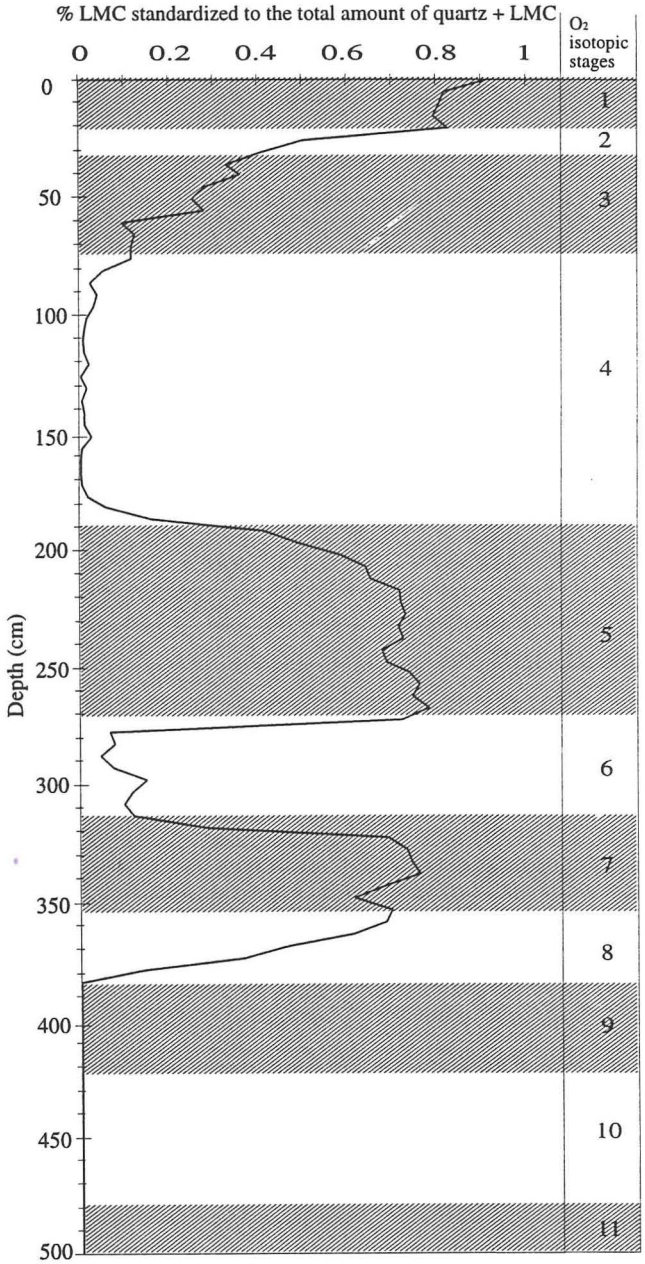

Fig. 4-14: LMC/quartz ratio of sediment core SO136-124GC. The percentage of calcite, standardized to the peak intensities of quartz and calcite is plotted against the core depth.

The graph shows increased calcite values during the interglacial stages 7, 5 and during the Holocene. Ca-values during the glacial periods converge towards zero. The extend to which the carbonate crust fragments (mentioned in chapter 4.5.

4.7. COALESCENS OF RESULTS

Although the plan was to correlate the sediment cores SO136-124GC and SO136-155GC, the results show, that this cannot be realized for the following reasons:

1.) the differences in depth from which the cores were retrieved are too large to compare both cores,

2.) the oceanographic regimes are different. Whereas core SO136-124GC is positioned slightly south of the Subantarctic Front and was retrieved from Subantarctic waters, the position of core SO136-155GC lies within the seasonal fluctuations of the Subtropical Front.

3.) As a result of this distribution of the core locations and the distinct depths, the lithologies of the investigated cores differ too much to perform an efficient correlation.

4.) The processes of sedimentation turned out to be of a completely different nature. The components of core SO136-124GC mostly consist of terrigenous material and of biogenic opal, the latter especially in the lower core section. Sedimentation through time is influenced by the fluctuations of the oceanographic front system and to a large extend by bottom currents and their erosional influence on the bathymetric high west of the core position.

Core SO136-155GC is strongly characterized by carbonate accumulation. Sedimentation in the past seems to have been steered by distinct bioproductivity due to paleoclimatic changes and by gravity slides coming down from the South Tasman Rise.

Due to these reasons the discussion for both sediment cores had to be carried out independently from each other. If possible or necessary, references are made.

5. DISCUSSION

5.1. SEDIMENT CORE SO136-124GC

5.1.1. The origin of the terrigenous material

Although the core position is located far away from any continental slopes, the sediments of this core consist mainly of terrigenous material (see chapter 4.6. MINERALOGY). The bathymetry and the bottom current system in this area have to be taken into account to determine the source of this terrigenous input. To the west, close to the core position a bathymetric high elevates to more than 1km above the surrounding seafloor (see fig. 5-1). Satellite altimetric data show, that the seafloor in this area has an average depth of 4000 - 4200m but the top of the high rises up to ~3000m below sea surface (Smith and Sandwell, 1997).

It is known that the area around the South Tasman Rise is an important passage for north-east heading deep and bottom water masses coming from westerly directions.

The South Tasman Rise (STR), as well as the bathymetric high, which might be a remainder of the submerged STR acts as an obstruction for the ACC deep and bottom currents. Due to this bathymetric high the currents are deflected around and over this feature eroding the structure during this process. The eroded material is transported downslope along the eastern flank of the high. As this is the leeward side, current energies are not high enough to continue the transport any longer and the material is sedimented at the bottom of the slope.

Evidence for this erosional process and the transport mechanisms are the terrigenous sediments found in sediment core SO136-124GC which was retrieved less than 10km east of this bathymetric feature (bottom topographic data taken from Smith and Sandwell, 1997).

Other evidence for this hypothesis is given by the high content of the fine fraction (40-90%) found throughout the entire SO136-124GC core (see section 4.5. WATER CONTENT AND % COARSE FRACTION). Strong bottom currents would have washed out a major part of the fine fraction. Therefore sedimentation must have occurred under minor bottom current energy conditions.

the bathymetric high while sedimentation takes place at the leeward, current-sheltered flank.

5.1.2. Correlation of the photospectrometry (700nm) and the SPECMAP-stack

As the $\delta^{18}O$ measurements on core SO136-124GC are not finished yet, a correlation of the 700nm curve with the SPECMAP stack (Imbrie et al., 1984) has been performed to obtain a first stratigraphic interpretation. At a later stage a uranium-thorium stratigraphy will follow (Rüggeberg, in prep.).
All spectra showed a good resolution (see section 4.3. SPECTROPHOTOMETRY).
The 700nm-curve was selected to correlate with the SPECMAP stack by Imbrie et al. (1984; fig. 5-2).
The 700nm curve of sediment core SO136-124GC could be correlated down to oxygen isotope stage 10. This corresponds to an age of approximately 385ka. The transition from stage 10 to 11 at 495cm core depth, the deepest sample investigated, is the oldest detectable signal. The correlation coefficient between the 700nm curve and the SPECMAP stack is 0.78.
Correlation has been definite for the Holocene and the transition to stage 2 (oxygen isotope stage 2 is represented by ~30cm of sediments). The signal for stage 3 is a bit unclear. A single peak at a core depth of 72cm is supposed to mark substage 3.3. The next certain markers are substages 5.1, 5.3 and 5.5 at core depth of ca. 200, 225 and 260cm, respectively.
The core interval from 75 to 190cm does not show any features except for some high frequent fluctuations which are interpreted as the current noise of the spectrophotometric data. If averaged, a gentle rise in values can be detected. However, with more than 9cm/ka the sedimentation rate during this interval (75-190cm) is too high to be of a "normal" pelagic nature (see section 5.1.3. SEDIMENTATION RATE AND BIOPRODUCTIVITY).
Oxygen isotope stages 6 to 10 could be correlated with the SPECMAP stack without major problems.

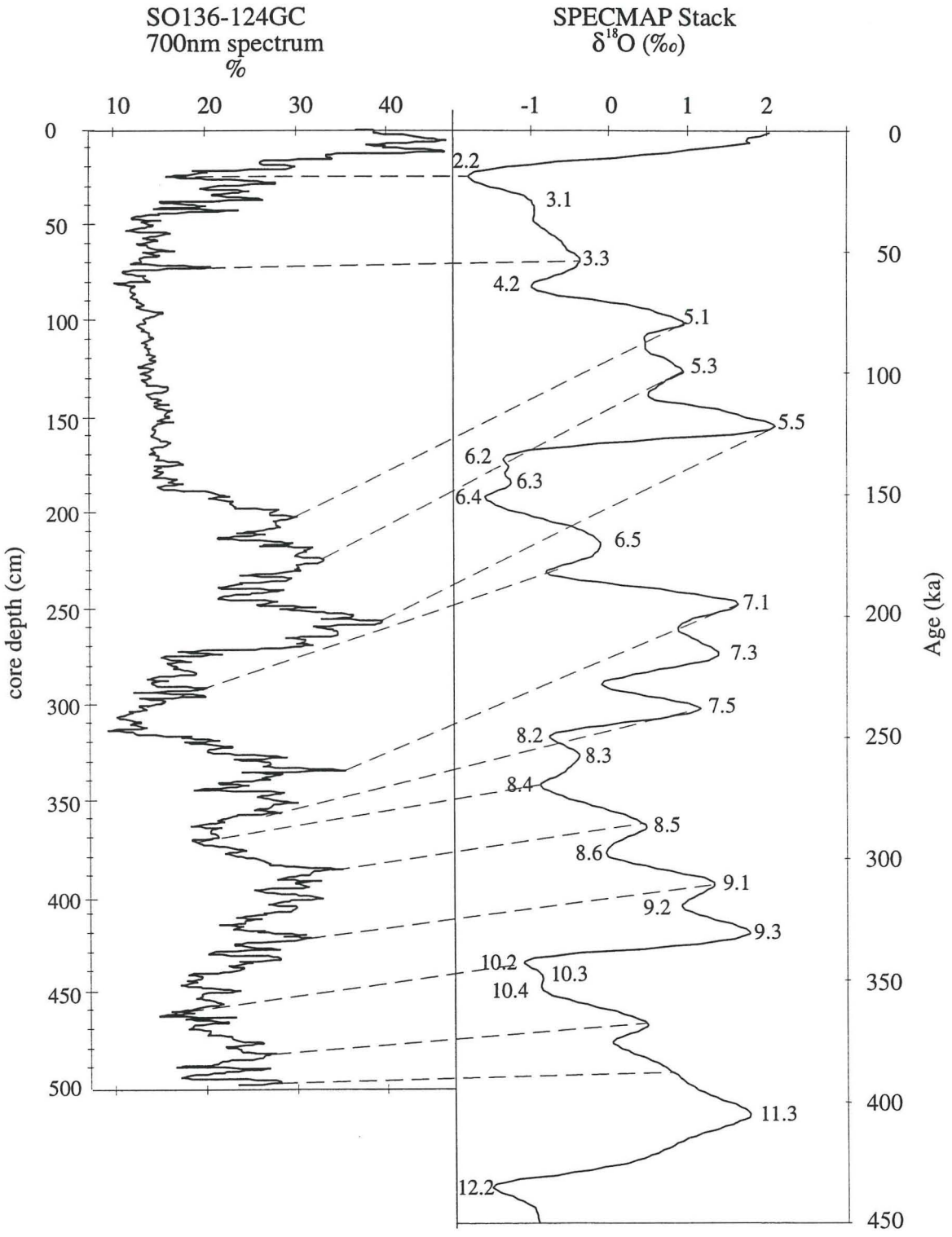

Fig. 5-2: Correlation of the 700nm spectrum with the SPECMAP stack (Imbrie et al.,1984). The correlation coefficient is 0.78.

5.1.3. Sedimentation rate and bioproductivity

Linear sedimentation rates show a pelagic sedimentation signal with increased terrigenous input throughout the entire core. An exception is represented in core section 75 to 190cm, which corresponds to oxygen isotope stage 4. This core section shows extraordinary high sedimentation rates of more than 9cm/ka. Although none of the analyses gave any proof for gravity induced mass slides, there must have been a process or an event that caused these high accumulation rates during this time.

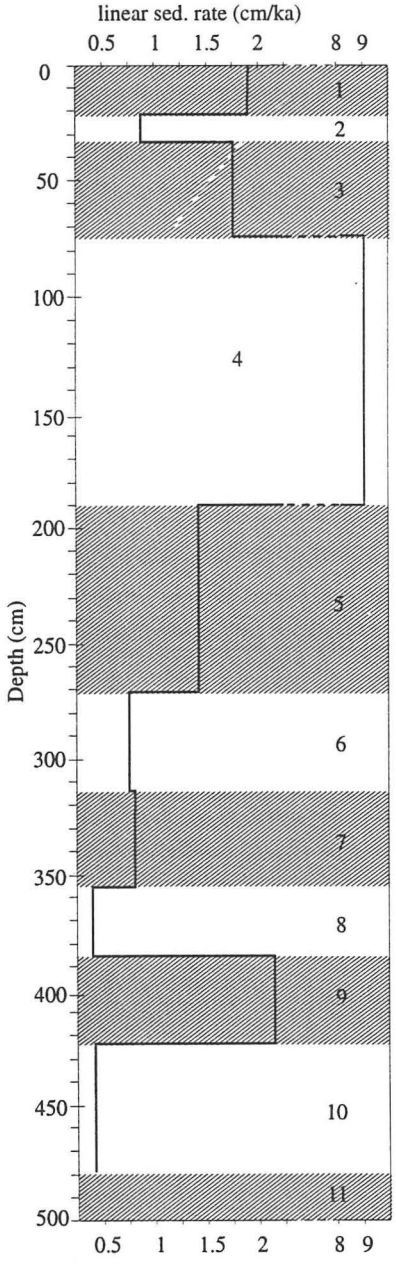

Fig. 5-3: Linear sedimentation rate of sediment core SO136-124GC.

In general, sedimentation rates show higher values for the interglacial periods and lower values for the glacials. As the amount of terrigenous input is assumed to have remained relatively stable (visual sample analysis), this distribution of the sedimentation signal is most likely a signal of changing bioproductivity. Increased bioproductivity during the interglacial stages is indicated by species with calcareous tests (mainly foraminifera) from core top down to stage 7. During the glacial stages, as well as below stage 7 the carbonate content converges towards zero, (see fig. 4-3) and siliceous components (diatom fragments, sponge spicules and radiolarians) form the main part of the biogenic sediment. Therefore, it can be concluded that carbonate production during the glacial stages was absent, or extremely low. Carbonate production during interglacial stages (up to stage 7) obviously was high enough to resist complete dissolution and to get into the sediment (see 5.1.6. The origin of the carbonate crusts).

At 310cm core depth, large radiolarians, the "so called fat rads" (pers. com. Thorsten Steiger, Munich, Germany), have their youngest appearance in this core. Below stage 7, the bioproductivity signal is replaced by changing production of biogenic opal (mainly diatom fragments and radiolarians). The amount of these "fat rads" increases and especially during the glacial periods 8 and 10 they build the main part of the coarse fraction.

The shift of the oceanographic frontal system is suggested to be the main factor having influenced the kind and amount of bioproduction. At present the core position is located slightly south of the Subantarctic Front (SAF). Therefore, carbonate production dominates (30 to 57% carbonate content during the Holocene). The carbonate contents are almost zero during the glacial stages and biogenic opal dominates the sediments. Thus, it is likely that the oceanographic frontal system shifted northward in the cold periods and core SO136-124GC became located south of the Polar Front (PF) within the influence of the biogenic opal belt surrounding Antarctica. The dominance of the biogenic opaline fraction in the sediments of glacial time spans would be the result from this dislocation. However, it is not known how far the oceanographic frontal system shifted northward within the glacial periods.

Figure 5-4 shows the proposed northward shift of the oceanographic frontal system over the core position of sediment core SO136-124GC.

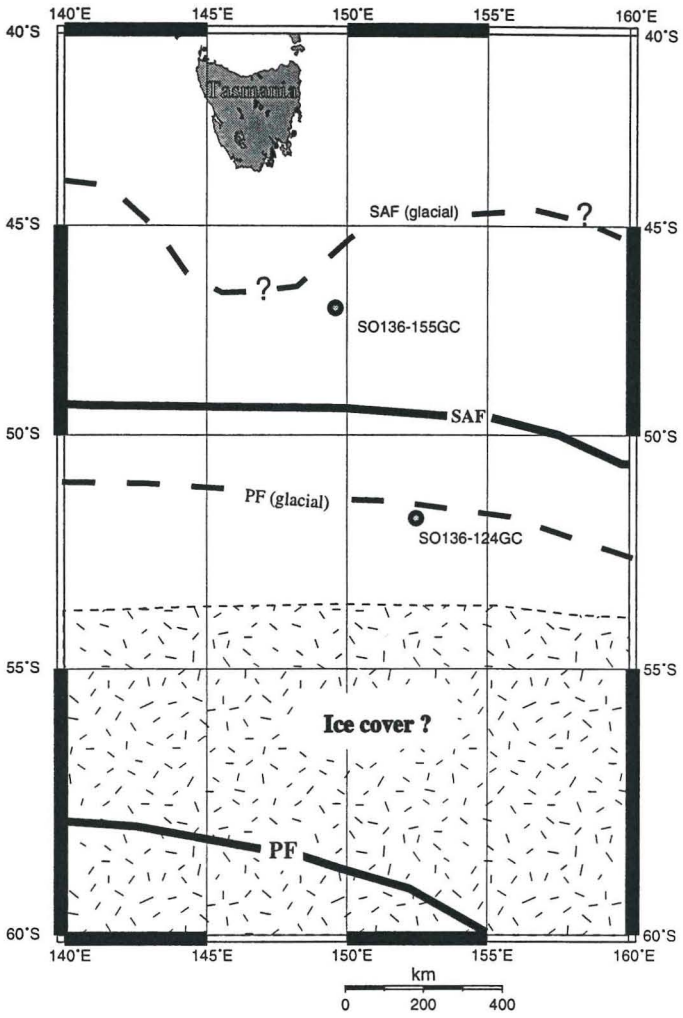

Fig. 5-4: Schematic map showing the proposed northward shift of the Polar Front (PF) and the Subantarctic Front (SAF) during glacial periods. Bold black lines show the present day positions of the PF and the SAF, dashed lines mark the presumed position of the fronts during the glacials. (positions of all fronts after Wells and Okada, 1996).

5.1.4. The manganese horizons

The ocean floor surrounding the position of core SO136-124GC is widespreadly covered by manganese nodules (SO136 cruise report, 1999).

Apart the manganese pavement at the sea-floor, two additional manganese horizons were discovered, at 30 and 360cm (see 4.1. LITHOLOGY). These manganese nodules are highly altered, which does not support the statement of Kennett (1982) that buried nodules remain unaltered at depth.

Both manganese horizons are positioned at transition phases from glacial to interglacial stages from, 2 to 1 and 8 to 7, respectively. Growth of the manganese nodules obviously occurred during glacial stages, whereas burial took place at the

beginning and during interglacial periods. This distribution allows the deduction, that sedimentation during glacial periods was small enough to allow growth of the manganese nodules whereas increased sedimentation during interglacial times buried these manganese horizons.

Whether low bioproductivity during these times is the main factor for low sedimentation or an increase in bottom current strength is not clear yet. Within the entire core the fine fraction content is high and thus decreased bioproductivity is more likely as a possible explanation for the burial of the nodules. The sedimentation rate variations within this core (except the feature between 75 and 180cm core depth) also favour changes in bioproductivity as a reason for the buried manganese horizons. Sedimentation rates remain relatively stable and follow the glacial and interglacial bioproductivity dependent distribution with increased bioproduction within the interglacials and decreased productivity during the glacials, respectively (see 5.1.3. SEDIMENTATION RATE). Additionally, no erosional surfaces have been detected.

Directly within the manganese horizon at 360cm a dropstone of ca. 1.5cm in diameter was found. This supports the theory, that these manganese nodules were exposed at the sediment surface during the glacial stage 8 and became buried at the onset of the following interglacial period (oxygen isotope stage 7).

5.1.5. The occurrence of ice rafted detritus (IRD)

It is not known yet how far north Antarctic icebergs did extend (pers. comm. Stefan Nees, GEOMAR, Kiel). Even if the Antarctic ice coverage did not extend as far north that it may have reached the investigated area, the IRD input shows that icebergs must have been moved over the core position. All of the dropstones occur at the ends of the glacial periods or at the transition phases from glacials to interglacials. Therefore, they correspond to the extensive melting phases at the end of the cold periods. More information of other cores in the investigated sea area will be needed to deduct the transport directions of these icebergs.

5.1.6. The origin of the carbonate crusts

The occurrence of the carbonate fragments as mentioned in section 4.5. (GRAIN SIZE DISTRIBUTION) and 4.6. (MINERALOGY), is a scientific problem which could not be totally solved within this thesis. It had to be known whether this bathymetric high is a fragment of the submerged STR and therefore, might have been under shallow water conditions during the Tertiary.

Nevertheless, three models will be proposed, which might be able to explain the occurrence and the distribution of the carbonate crust fragments.

There are five intervals in which these carbonate fragments occur, at 195, 285, 320, 335 and 380cm core depth.

All of these depths correspond either to the end of an interglacial period or to the transition from glacial to interglacial periods e. g. core depth 380cm (transition from stage 9 to stage 8), 320cm (transition from stage 7 to stage 6), and 195cm (transition phase from stage 5 to stage 4). The carbonate fragments at 285cm occur at the end of stage 6. The 335cm carbonate detritus horizon is positioned well within oxygen isotope stage 7.

The $\delta^{18}O$ analyses show values from -4.3 to -13.2‰ and the $\delta^{13}C$ values range from -2.8 to - 9.1‰. The wide range of the values measured shows that diagenesis occurred and that no interpretation can be made using the $\delta^{18}O$ and $\delta^{13}C$ measurements. A possible explanation for the results of the $\delta^{18}O$ and $\delta^{13}C$ analysis is the leached state (due to decalcification) of the fragments. Only a weak reaction on the treatment of calcium carbonate with HCl could be observed.

The following model is one proposition to explain the formation and deposition of these carbonate crusts. Changing corrosiveness of the sea water due to glacial and interglacial changes might have played a major role in this diagenetic process.

Due to high pressure, low temperature and high CO_2 partial pressure the ocean is undersaturated with respect to $CaCO_3$ in the deep waters of this ocean area (Martínez, 1992).

Due to the northward shift of the oceanographic frontal system during the glacials, bioproduction was dominated by siliceous material and no carbonate was produced.

Within the interglacial stages, bioproduction was dominated by species producing calcareous tests, e.g. foraminifera and calcareous nannoplankton. Due to increased carbonate production at the onset of the warm periods and subsequent dissolution,

the sea water gets more saturated in comparison with glacial waters. As a result the CCD deepens during the interglacials. When the CCD finally reaches the seafloor (4200m at core position), precipitation of $CaCO_3$ is possible and its deposition as calcareous ooze occurs at the seafloor.

Within the transition phase from interglacials to glacials the sea surface water temperature decreases, the frontal system shifted northward and the bioproduction of calcareous tests decreases. As a consequence the water masses become undersaturated again and the CCD moves up to a level somewhere in the water column. At these time periods, the seafloor at the core position was below the CCD and the previously precipitated material at the sediment surface is partly solved again (leached). Dissolution by the sea water decreases or ends when the calcareous oozes get covered by sediment. The leached carbonate remains in the sediment column and becomes "half way lithified" by diagenetic processes. This hypothesis may explain the occurrence of the carbonate crusts at the specific positions within the interglacial time periods and at the transition phases between interglacial and glacial times. However, the occurrence of the crust fragments at 285cm core depth (within stage 6) remains unclear.

Other uncertainties are the unknown influence of pore water within the sediment column as well as the process that is responsible for the fragmentation of these carbonate crusts.

A second possibility for the origin of the crusts might be their formation on top of the rise west of the core position during the warmer interglacial periods and their subsequent downslope transport. This would give evidence for the fragmentation of the former half lithified carbonate crusts but is unlikely to explain the periodic occurrence of the carbonate crust levels within the sediment core.

A third hypothesis deals with the age of these carbonate fragments. Possibly, they are older than Quaternary and were built as shelf carbonates somewhen during the Tertiary, before the STR submerged. Evidence is given by dredged samples from the South Tasman Rise during the SONNE cruise SO36 (3rd Leg), which were supposed to be older than Tertiary (SO36 cruise report, 1985). After sedimentation at the still shallow shelf they became (half way) lithified and submerged with the STR. Subsequent erosion by bottom and deep water currents would have exposed these sediments and would have eroded them afterwards (see section 5.1.1. ORIGIN OF THE TERRIGENOUS MATERIAL). This model would allow to explain the occurrence of the carbonate as fragments or detritus as a result

of downslope transport. However the distinct periodicity of the input would be a question remaining unsolved.

5.2. SEDIMENT CORE SO136-155GC

Unlike core SO136-124GC, this core shows almost no terrigenous components. The sediments are dominated by carbonate material, composed mainly of foraminiferal sands and foram-bearing to foram marl oozes.
Carbonate content varies from 81 to 91% (see 4.2. $CaCO_3$ - ANALYSIS).
The spectrophotometric data and logging analysis (WBD & MS) show good resolution down to upper stage 6 allowing a precise classification into glacial and interglacial time periods (see chapters 4.3. & 4.4.).
The distribution of % coarse fraction does not provide much information except for the negative peak within core section 295 - 310cm indicating the foram ooze layer on top of the upper turbidite.
Out of the five subfractions after dry sieving, the subfractions 63-125µm and 250-500µm showed a clear productivity signal (see fig. 4-11), which will be interpreted later within this section (5.2.2. Bioproductivity and sedimentation rate).
The XRD analysis proved the non-existence of HMC. LMC is the dominant component throughout the entire core and quartz shows extremely low values (see fig. 4-15 and 4-16 and following discussion).

5.2.1. The mineral contents

The mineralogy within core SO136-155GC is very monotonous. LMC is by far the most common component. A very small amount of quartz could be detected (see 4.6. MINERALOGY). These two minerals are by far the most dominant components detectable using X-ray diffraction. The occurrence of halite is a residue of dried pore water within the samples (see section 4.6. MINERALOGY).
There is no indication for HMC throughout the entire core. This is probably due to the core location being too far away from the continental shelf of Tasmania. The bathymetric saddle in between Tasmania and the STR acts as a sediment trap that cannot be bypassed by gravity induced sediment deposits like slides, slumps or turbidite currents which might transport HMC from the Tasmanian shelf.

Foraminifera build the main part of these sediments within the upper core section of non-turbidite sedimentation, as well as within the section of turbidite sedimentation. No major changes in mineralogy can be observed throughout the entire core. Only some changes in the quartz – LMC ratio can be detected (see fig. 4-16). These fluctuations are due to thinning of the quartz by LMC during periods of increased bioproduction within the interglacial time spans. During the glacials an increased quartz signal can be observed due to a slightly decreased carbonate production (see section 5.2.2. BIOPRODUCTION AND SEDIMENTATION RATE).

5.2.2. Bioproduction and sedimentation rate

The large portion of biogenic components in the sediment allows to suggest that fluctuations in bioproductivity is the major effect controlling the sedimentation of this sediment core. The grain size distribution of the subfractions >63µm (especially the fractions 63-125µm and 250-500µm, which consists mainly of foraminifers) give a first idea of the paleoproductivity. Increased values of the finest coarse fraction during the interglacials indicate periods of increased calcareous bioproduction, whereas the glacial time spans show increased values in the subfraction 250-500µm and a decreased in the amount of the 63-125µm subfraction. Even the substages within the interglacials can be traced (see section 4.5.).

The sedimentation rate remains medium throughout the entire core (2-2.5cm/ka) with the higher values during the interglacials (2.4-2.5cm/ka) and lower values (~2cm/ka) within stages 2-4. Increased calcareous bioproduction during the interglacial time periods is thought to be the major reason for an increased sedimentation rate. In addition, the turbidite sedimentation within the lower core section from 290-500cm shows that bioproduction must have been very high below stage 6.

Figure 5-5 shows the linear sedimentation rate of sediment core SO136-155GC.

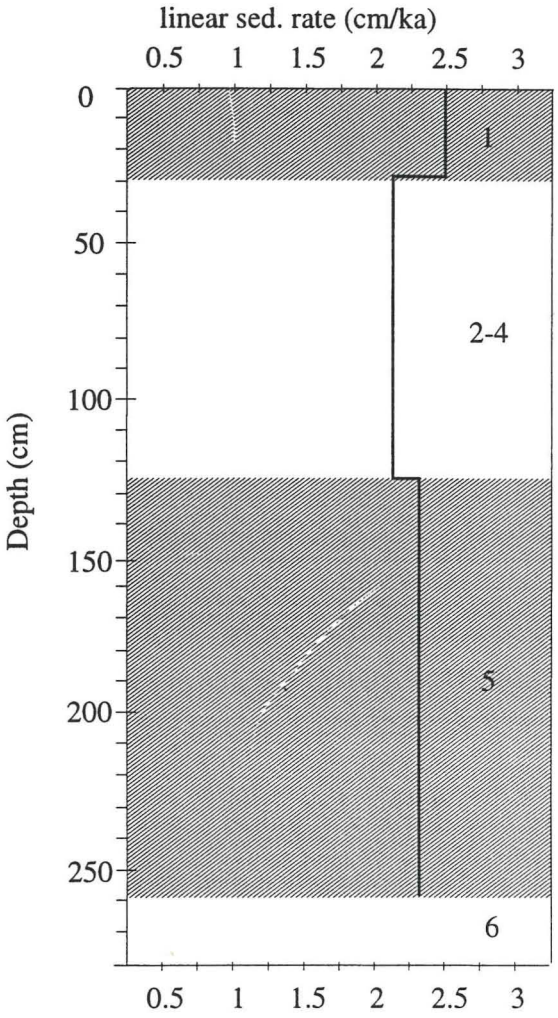

Fig. 5-5: Linear sedimentation rate of sediment core SO136-155GC for the upper 280cm.

5.3. PALEOCEANOGRAPHIC INTERPRETATION

The signals of bioproductivity and dissolution show remarkable differences within both sediment cores. Whereas dissolution seems to have been stronger during the glacials in core SO136-124GC, the spectrophotometrical data of core SO136-155GC give evidence for an increased dissolution during interglacial periods. The processes controlling the grade of dissolution must be of a different character. To explain this feature, the geographic positions and their oceanographic background should be considered.

At present the position of core SO136-124GC is located south of the Subantarctic Front (see fig. 5-4) and today carbonate production is dominating. Evidence gives the high carbonate content within the upper section representing the Holocene

(see section 4.2. $CACO_3$ ANALYSIS). During glacial times the oceanographic frontal system may have shifted northward and the core position then must have been located around or slightly south of the Polar Front (see fig. 5-4). Due to the influence of the biogenic opal belt, surrounding Antarctica, production of siliceous material dominated within the glacials. As biogenic carbonate production was absent or very low in this specific area and surface water temperature was lower than during the interglacials, the sea water became supersaturated with respect to CO_3^{2-}. As a consequence, the lysocline and the CCD subsequently lowered and $CaCO_3$ was dissolved. Evidence for this process gives the carbonate curve which shows high carbonate values during interglacials whereas carbonate is absent during the glacials (see fig. 4-3). If the corrosiveness of the Antarctic Bottom Water-influenced bottom and deep waters in this area is assumed to have been relatively stable, dissolution and therefore carbonate preservation patterns are mainly controlled by changing carbonate production. Thus dissolution was stronger during the glacials and weaker within the interglacials. This feature has already been described for the Tasman Sea Area by Martínez (1994).

In contrast, dissolution patterns within core SO136-155GC operate under another mechanism. The present core position is located south of the Subtropical Front within the Subantarctic Zone which is a high production area. It is assumed that the northward shift of the oceanographic frontal system was hindered by the continental shelf of Tasmania and thus the oceanographic zones were thinned (Wells and Okada, 1996). Most probably the core location was not affected by this shift and stayed within the Subantarctic Zone throughout the Late Quaternary. Therefore, carbonate contents are very high (81-91%) throughout the entire core (see fig. 4-3). Due to increased dissolution the spectrophotometric data show lighter values during the interglacial stages. This is a consequence of increased input of biomass during the interglacials. Increased respiration by organisms and oxidation of calcareous tests cause an enhanced CO_2 partial pressure. The CO_2 partial pressure is, beneath hydrostatic pressure, carbonate ion content and temperature of the sea water, a major factor controlling dissolution of calcium carbonate (Kennett, 1982). With the increase of CO_2 partial pressure, dissolution increases. Therefore, dissolution in this ocean area was stronger during interglacial time periods.

The big differences in dissolution patterns between the two cores investigated seems to be surprising. However, previous investigations of sediment cores in the Tasman Sea showed that local surface organic productivity may account for

geographical variations in dissolution and fragmentation patterns (Martínez, 1994). In addition, metabolic oxidation of organic matter in the pore waters of sediments located below the lysocline may enhance dissolution of carbonaceous tests (Emerson and Archer, 1992). Therefore, variations of dissolution and fragmentation patterns within the same ocean region seems to be a common feature in the investigated sea area.

The position of the CCD through time cannot be deduced precisely by the results of the sediment cores investigated. Per definition, the CCD is the depth above which carbonate-rich sediments accumulate and below which carbonate-free sediments accumulate (Kennett, 1982). Therefore, it can be stated that the CCD in the sea area of core SO136-124GC was definitely deeper than 4170m during the interglacials while it might have been somewhere shallower in the water column within the glacials. The ocean floor at the core position of SO136-155GC definitely was above the CCD throughout the stages 1 to 6.

The common occurrence of dropstones within sediment core SO136-124GC shows that several icebergs must have been moved over the core position. It has to be assumed that the icebergs did extend further north than thought in the past (evidence gives the subfraction >1000µm and the X-raying of the sediment).

6. CONCLUSIONS

- Sediment core SO136-124GC shows pelagic sedimentation with extraordinary high terrigenous input. The terrigenous material is derived from the bathymetric high west of the core position. Due to westerly bottom and deep water currents flowing over and around this elevation, the terrigenic components are eroded and transported downslope along the eastern flank. At the leeward, current sheltered side, current strength is not high enough to continue the transport any longer and the terrigenous material is sedimented. In addition, three manganese horizons were present, which became buried at the transition from glacial to interglacial stages. The occurrence of several levels of carbonate crusts could not be completely cleared within this thesis. However some models are proposed which might be able to explain the formation and deposition of these carbonate crust fragments.
Core SO136-155GC is dominated by highly carbonaceous sediments, containing mainly foram sands and foram marl oozes.

- As a result of the northward shift of the oceanographic front system the core position of core SO136-124GC was located south of the Subantarctic Front (SAF) during the interglacials and slightly south or around the Polar Front (PF) during the glacials. As a consequence of this, the biogenic production of interglacial times is dominated by carbonate components whereas the glacials are characterized by siliceous bioproduction.
Core SO136-155GC is supposed to have remained within the highly carbonate productive Subantarctic Zone and was not affected by the shift of the oceanographic frontal system. Therefore, its sediments are dominated by carbonate throughout the entire core.

- The sedimentation rate of core SO136-124GC varies from 0.3 to 2.4cm/ka with the higher values during the interglacials (0.8-2.3cm/ka) and lower values within the glacials (0.3-0.7cm/ka).
Core SO136-155GC shows sedimentation rates from 2cm/ka during stages 2-4 and 2.4 to 2.5cm/ka for stage 5 and the Holocene, respectively. Sedimentation in both cores is mainly controlled by changing bioproductivity as a signal of glacial and interglacial changes.

- Dissolution patterns are largely determined by local productivity levels. In the area of core SO136-124GC dissolution was stronger during glacials. Due to increased production and input of calcareous tests within the interglacials (shift of the oceanographic frontal system) dissolution was less within these time periods. Dissolution patterns for core SO136-155GC are distinctly different. Due to increased bioproduction, respiration by organisms and oxidation of calcareous tests enhances the CO_2 partial pressure. As a consequence, dissolution is stronger within the interglacials and less during the glacials, respectively.

The variability of dissolution and fragmentation patterns within this ocean area does neither correspond to the Atlantic Ocean mechanisms, nor to those of the Pacific Ocean. This may show the importance of the investigated ocean sector as a link between the Atlantic, Indian and Pacific Oceans. A better knowledge of the Southern Ocean might therefore provide valuable information to understand the processes in the world oceans.

ACKNOWLEDGEMENTS

I thank Prof. Dr. W.- Chr. Dullo for making the performance of this thesis at GEOMAR possible.

Thanks to the shipboard party of the RV SONNE cruise SO136 for enjoyable weeks on board during the October and November 1998.

I wish to thank my colleagues Arne Sturm, Terry Mills and especially Andres Rüggeberg for the good and pleasant team-work while this thesis came into existence.

Special thanks to my Irish friend Dr. Brian Ward (Nansen environmental and Remote sensing Centre, Bergen, Norway) for checking my English and getting rid of millions of unnecessary commas.

I'm grateful to Dr. Stefan Nees for spending his limited time for valuable discussions and for reviewing this thesis.

I thank John J. G. Reijmer for being a grand supervisor, supporting me in any respects. I'm looking forward to further team work.

Finally, many thanks to my grandparents and parents for their patience and their generous support throughout my studies.

REFERENCES

Andruleit, H. A. & Baumann, K.-H. (1998) History of the last Deglaciation and Holocene in the Nordic seas as revealed by coccolithophore assemblages. Marine Micropaleontology, 35, 179-201.

Assallay, A. M., Rogers, C. D. F., Smalley, I. J. & Jefferson, I. F. (1998) Silt: 2 - 62μm, 9 - 4 Phi. Earth-Science Reviews, 45, 61-88.

Bareille, G. (1991) Flux sedimentaires: paléoproductivité et paléocirculation de l'Océan Austral au cours des 150.000 dernières années. PhD Thesis, Université de Bordeaux.

Barranco, F. T. j., Balsam, W. L. & Deaton, B. C. (1989) Quantitative reassessment of brick red lutites: evidence from reflectance spectrophotometry. Marine Geology, 89, 299-314.

Boreen, T. D. & James, N. P. (1993) Holocene sediment dynamics on a cool-water carbonate shelf: Otway, Southeastern Australia. Journal of sedimentary Petrology, 63(4), 574-588.

Camoin, G. F. & Davies, P. J. (1998) Reefs and Carbonate Platforms in the Pacific and Indian Oceans, pp. 328. Blackwell Science Ltd, Oxford.

Cochran, J. K. & Osmond, J. K. (1976) Sedimentation patterns and accumulation rates in the Tasman Basin. Deep-Sea Research, 23(3), 193-210.

Conolly, J. R. A. P., Robert R. (1972) Sedimentary Patterns within a Continent-Mid-Oceanic Ridge-Continent Profile: Indian Ocean South of Australia. In: Antarctic Oceanology II, Vol. 19 (Ed. by D. E. Hayes), pp. 295-315. American Geophysical Union. Antarctic Research Series.

De Deckker, P. (1997) The significance of the oceans in the Australasian region with respect to global palaeoclimates: future directions. Palaeogeography, Palaeoclimatology, Palaeoecology, 131, 511-515.

Dietrich, G., Kalle, K., Krauss, W. & Siedler, G. (1975) Allgemeine Meereskunde. III Aufl., Gebrüder Bornträger, Berlin, Stuttgart, 593 pp.

Dulk den, M., Reichart, G. J., Memon, G. M., Roelofs, E. M. P., Zachariasse, W. J. & van der Zwaan, G. J. (1998) Benthic foraminiferal response to variations in surface water productivity and oxygenation in the northern Arabian Sea. Marine Micropaleontology, 35, 43-66.

Ehrlich, L. H. (1998) Geomicrobiology: its significance for geology. Earth-Science Reviews, 45, 45-60.

Exon, N. F., Marshall, J. F., McCorkle, D. C., Alcock, M., Chaproniere, G. C. H., Connell, R., Dutton, S. J., Elmes, M., Findlay, C., Robertson, L., Rollet, N., Samson, C., Shafik, S. & Whitmore, G. P. (1995) AGSO Cruise 147 Report - Tasman Rises Geological Sampling Cruise of Rig Seismic: stratigraphy, tectonic and palaeoclimate of the offshore Tasmanian Region. AGSO Record, 1995/56, 159.

Exon, N. F., Royer, J.-Y. & Hill, P. (1996) Tasmanate cruise: swath-mapping and underway geophysics south and west of Tasmania. Marine Geophysical Researches, 18(1996), 275-287.

Füchtbauer, H. (1988) Sedimente und Sedimentgesteine, Sediment-Petrologie Teil II. Schweizerbart'sche Verlagsbuchhandlung, Stuttgart, 1141 pp.

GEOTEK (1998) Manual: Multi Sensor Core Logger. Daventry, UK.

Gordon, A. L. (1972) On the interaction of the Antarctic circumpolar current and the Macquarie Ridge. In: Antarctic Oceanology II, The Australian - New Zealand Sector, Vol. 19 (Ed. by D. E. Hayes), pp. 71-78. American Geophysical Union, Washington.

Hayes, D. E. & Ringis, J. (1973) Seafloor spreading in the Tasman Sea. Nature, 243, 454-458.

Hesse, P. P. (1997) Mineral magnetic "tracing" of aeolian dust in southwest Pacific sediments. Palaeogeography, Palaeoclimatology, Palaeoecology, 131, 327-353.

Hinz, K. & sientific shipboard party (1985) Geophysical, geological and geochemical studies off West Tasmania and on the South Tasman Rise. Bundeanstalt für Geowissenschaften und Rohstoffe, Cruise Report SO 36B.

Hiramatsu, C. & De Deckker, P. (1997) The late Quaternary calcareous nannoplankton assemblages from three cores from the Tasman Sea. Palaeogeography, Palaeoclimatology, Palaeoecology, 131, 391-412.

Imbrie, J., Hays, J. D., Martinson, D. G., McIntyre, A., Mix, A. C., Morley, J. J., Pisias, N. G., Prell, W. L. & Shackleton, N. J. (1984) The orbital theory of Pleistocene climate: support from a revised chronology of the marine $\delta\ ^{18}O$ record. In: Milankovitch and Climate, Vol. C126(I) (Ed. by A. Berger, J. Imbrie, J. Hays, G. Kukla and B. Saltzman), pp. 269-305. Reidel, NATO Series, Netherlands.

James, N. P. & Bone, Y. (1991) Origin of cool-water, Oligo-Miocene deep shelf limestone, Eucla Platform, southern Australia. Sedimentology, 38, 323-341.

James, N. P. & Clarke, J. A. D. (1997) Cool-Water Carbonates. SEPM, Tulsa.

Kennett, J. P. & Shackleton, N. J. (1976) Oxygen isotopic evidence for the development of the psychrosphere 38 Myr ago. Nature, 260, 513-515.

Kennett, J. P. (1978) The development of planktonic biogeography in the Southern Ocean during the Cenozoic. Marine Micropaleontology, 3, 301-345.

Kennett, J. P. (1982) Marine Geology. Prentice Hall Inc., Englewood Cliffs, N.J., 813 pp.

Klinck, J. M. & Smith, D. A. (1993) Effect of wind changes during the last glacial maximum on the circulation in the Southern Ocean. Paleoceanography, 8, 427-433.

Kumar, N., Anderson, R. F., Mortlock, R. A., Froelich, P. N., Kubik, P., Dittrich-Hannen, B. & Suter, M. (1995) Increased biological productivity and export production in the glacial Southern Ocean. Nature, 378, 675-680.

Labeyrie, L., Labracherie, M., Gorfti, N., Pichon, J. J., Vautravers, M., Arnold, M., Duplessy, J.-C., Paterne, M., Michel, E., Duprat, J., Caralp, M. & Turon, J.-L. (1996) Hydrographic changes of the Southern Ocean (southeast Indian sector) over the last 230 kyr. Paleoceanography, 11(1), 57-76.

Martínez, J. I. (1994) Late Pleistocene palaeoceanography of the Tasman Sea: implications for the dynamics of the warm pool in the western Pacific. Palaeogeography, Palaeoclimatology, Palaeoecology, 112((1994) 1-2), 19-62.

Martínez, R. J. I. (1997) Decreasing influence of Subantarctic Mode Water north of the Tasman Front over the past 150 kyr. Palaeogeography, Palaeoclimatology, Palaeoecology, 131, 355-364.

Martínez, J. I., De Deckker, P. & Barrows, T. T. (1999) Paleoceanography of the last glacial maximum in the eastern Indian Ocean: planktonic foraminiferal evidence. Palaeogeography, Palaeoclimatology, Palaeoecology, 147, 73-99.

Nagao, S. & Nakashima, S. (1992) The factors controlling vertical color variations of North Atlantic Madeira Abyssal Plain sediments. Marine Geology, 109, 83-94.

Nees, S., Jellinek, T., Suhonen, J., Winkler, A., Helmke, J. & Emmermann & scientific shipboard party (1998) Cruise Report: Images III - IPHIS (Indian and Pacific Ocean Pleistocene and Holocene History: an IMAGES Study).

Orsi, A. H., Whitworth III, T. & Worth, D. N. J. (1995) On the meridional extent and fronts of the Antarctic Circumpolar Current. Deep-Sea Research I, 42(5), 641-673.

Pickering, K. T., Hiscott, R. N. & Hein, F. J. (1989) Deep marine environments: Clastic sedimentation and tectonics. Unwin Hyman Inc., London, 416 pp.

Pinxian, W. (1999) Response of Western Pacific marginal seas to glacial cycles: paleoceanographic and sedimentological features. Marine Geology, 156, 5-39.

Rao, P. C. & Amini, Z. Z. (1995) Faunal relationship to grain-size, mineralogy and geochemistry in recent temperate shelf carbonates, Western Tasmania, Australia. Carbonates and Evaporates, 10(1), 114-123.

Rey, J. (1991) Geologische Altersbestimmungen. Ferdinand Enke Verlag, Stuttgart, 195 pp.

Rintoul, S. R., Donguy, T. R. & Roemmich, D. H. (1997) Seasonal evolution of upper ocean thermal structure between Tasmania and Antarctica. Deep-Sea Research I, 44(7), 1185-1202.

Smith, W. H. J. & Sandwell, D.T. (1997) Global seafloor bathymetry from satellite altimetry and ship depth soundings. Science, 272, 1956-1962.

Suhonen, J. M. (1998) Mineralogy, sedimentology and physical properties of core MD 97-2108 (South Tasman Rise, Tasman Sea). Masters Thesis, University of Helsinki, 51 pp.

Thiede, J. (1979) Wind regimes over the late Quaternary southwest Pacific Ocean. Geology, 7, 259-262.

Thiede, J., Nees, S., Schulz, H. & De Deckker, P. (1997) Oceanic surface conditions recorded on the sea floor of the Southwest Pacific Ocean through the distribution of foraminifers and biogenic silica. Palaeogeography, Palaeoclimatology, Palaeoecology, 131, 207-239.

Thompson, R. O. R. Y. & Edwards, R. J. (1981) Mixing and Water-Mass Formation in the Australian Subantarctic. Journal of Physical Oceanography, 11(10), 1399-1406.

Tomczak, M. & Godfrey, J. S. (1994) Regional Oceanography: an introduction. Pergamon, Oxford, 422 pp.

Tucker, M. (1988) Techniques in Sedimentology. Blackwell Scientific Publications, 394 pp.

van der Lingen, G. J., Swanson, K. M. & Muir, R. J. (1994) The evolution of the Tasman Sea basin, pp. 261. Balkema, Rotterdam.

Weber, M. E. (1998) Estimation of biogenic carbonate and opal by continuous non-destructive measurements in deep-sea sediments: application to the eastern Equatorial Pacific. Deep-Sea Research I, 45, 1955-1975.

Wells, P. E. & Okada, H. (1996) Holocene and Pleistocene glacial palaeoceanogrphy off Southeastern Australia, based on foraminifers and nannofossils in Vema cored hole V18-222. Australian Journal of Earth Sciences, 43, 509-523.

Wells, P. E. & Conell, R. (1997) Movement of hydrological fronts and widespread erosional events in the southwestern Tasman Sea during the Late Quaternary. Australian Journal of Earth Sciences, 44, 105-112.